Restricted **SR.15.11616**

Geomechanical experiments on Ten Boer rock samples from well Moddergat-3

by

A.J. van der Linden (PTI/RF)

P.M.M. Zuiderwijk (PTI/RF)

S. Hol (PTI/RF)

F. Marcelis (PTI/RF)

A.H. Coorn (PTI/RF)

Shell Global Solutions International B.V., Rijswijk

Further electronic copies can be obtained from the Global Information Centre.

Executive summary

The research reported here was carried out in the framework of a long-term Subsidence Study (High Order Subsidence Monitoring project (HOSM project)), supervised by the Royal Dutch Academy of Science (KNAW) and executed by NAM.

In order to aid our understanding of subsidence, and its underlying mechanisms, of selected Wadden Sea areas, we have characterized the mechanical behaviour of Ten Boer cap rock material, taken from well Moddergat-3 (Nes gas field, The Netherlands). We have subjected 14 plugs sub-sampled from the cores to pore pressure depletion under uniaxial strain boundary conditions on fourteen samples (8 shaly sandstone and 6 shale samples).

All pore pressure depletion tests started from in-situ stress conditions (S_{ax}: 80 MPa, S_{rad}: 67 MPa, P_{pore}: 57 MPa) and reached the anticipated maximum depletion conditions (P_{pore}:3 MPa) in 35 to 300 hours depending on the applied test procedure. Six samples were also subjected to inflation under uniaxial strain conditions.

The mechanical response of the caprock was parameterized by assuming the validity of linear poroelasticity, and resulted in the following:

	shaly sandstone	Shale (Ppore : 57 – 47 MPa)
Young's modulus	19.9 ± 3.9 GPa	12.8 ± 1.7 GPa
Poisson's ratio.	0.09 ± 0.03	0.04 ± 0.03
Depletion constant γ	0.88 ± 0.04	0.95 ± 0.04

It should be noted that approximately 30% of the depletion-induced deformation was non-recoverable. Moreover, shear failure has been observed during the pore pressure depletion steps for five of the six pure shale samples. All shaly sandstone samples remained intact during the depletion steps.

Table of contents

Executive summary II
1. Introduction 1
2. Methods 2
2.1. Sample and pore fluid preparation 2
2.2. Experimental conditions and procedures. 3
2.2.1. Shaly sandstone samples *4*
2.2.2. Shale samples *5*
2.3. Data processing 6
3. Results 7
3.1. Pore pressure depletion data shaly sandstone streaks 7
3.2. Tests with samples from shale material 12
4. Summary of key observations 18
References 19
Appendix 1. Photographs and CT scans of Ten Boer samples. 20
Appendix 2. Test results. 37
Appendix 3. Experimental setup 43
Bibliographic information 45
Report distribution 46

List of figures

Figure 1: Example of depletion-inflation stress path for shaly sandstone samples. 5
Figure 2: Stress as a function of time for the stepwise depletion path. 6
Figure 3: CT scan of post-test sample MGT3-2A. 9
Figure 4: Sample MGT3-17B: stress-strain curve for pore pressure depletion step (P_{pore}: 17 MPa to 7 MPa). 13
Figure 5: Sample MGT3-17B: CT scan of pre-test (left) and post-test (right) sample. 14
Figure 6: Evolution of the Young's modulus parameterized from measured stress-strain response during the pore pressure depletion steps for the Ten Boer shale samples. 15
Figure 7: Depletion constant parameterized on the basis of the change in radial stress and pore pressure measured during depletion for all samples, and plotted versus pore pressure depletion change. 15
Figure 8: The Young's modulus, parameterized from measured stress-strain response, plotted versus sample depth of the Ten Boer shale samples. The Young's modulus were determined during for the first (P_{pore} = 57 MPa to 47 MPa) and second (P_{pore} = 47 to 37 MPa) pore pressure depletion step. 16

List of tables

Table 1: Composition of artifial brine 2
Table 2: Samples, depth and lithology used for pore pressure depletion tests 3
Table 3: In-situ stress for Moddergat-3. 4
Table 4: Overview of test samples applying the depletion-inflation stress path and the pore pressure change during depletion. 5
Table 5: Samples drilled from the shaly sandstone layers, their depth and depletion range. 7
Table 6: Young's modulus and Poisson's ratio determined in the axial loading step to in-situ axial total stress (shaly sandstone samples). 8
Table 7: Average Young's modulus, Poisson's ratio and depletion constant of the shaly sandstone tests determined in the first depletion step. 10
Table 8: Results of the pore pressure depletion tests with shaly sandstone samples from the Ten Boer formation applying the stepwise depletion stress path (Figure 2). 11
Table 9: Results of the pore pressure depletion tests with shaly sandstone samples from the Ten Boer formation applying the pore pressure depletion-inflation stress path (Figure 1). 11
Table 10: Young's modulus and Poisson's ratio determined in the axial loading step to in-situ axial total stress (shale samples). 12
Table 11: Results of the pore pressure depletion experiments with shale samples from the Ten Boer formation. 17

LIST OF ABBREVIATIONS AND SYMBOLS

C_m Uniaxial compressibility (also termed uniaxial compaction coefficient), defined as the compaction strain along the cylindrical axis (ε_a) of the sample per unit increment of effective axial stress (σ_a) under zero radial displacement (MPa^{-1})

K Bulk modulus (GPa)

K_s Bulk modulus of grains (GPa)

P_{pore} Pore-fluid pressure (MPa)

S_{rad} Total radial stress (MPa)

S_{rad}' Effective radial stress (MPa), defined as the difference between total radial stress and pore-fluid pressure, i.e. assuming Terzhagi effective stress.

S_{ax} Total axial stress (MPa)

S_{ax}' Effective axial stress (MPa), defined as the difference between total axial stress and pore-fluid pressure, i.e. assuming Terzhagi effective stress.

ε_a Axial strain

γ Depletion coefficient ($\Delta S_{rad}/\Delta P_{pore}$)

α Biot-Willis coefficient

1. Introduction

Production-induced subsidence is a concern to the North Netherlands because of the position relative to sea level. Aside from the spatial nature of subsidence, also temporal effects must be considered, and thus the question whether subsidence will continue after production has stopped. In the last decades, experimental work has focussed on creep deformation in reservoir material only [1] [2]. The outcome of these studies has been used to predict the subsidence in north-east Netherlands.

In 2012, well Moddergat-3 was drilled by NAM (Nederlandse Aardolie Maatschappij) for production from gas fields Nes and Moddergat which are partly located underneath the Wadden Sea. 110 Meter of core material was retrieved and send to the Shell Rock and Fluids laboratories in Rijswijk for experimental study. The main focus of the experimental programs on the core material has been on the Rotliegendes reservoir material [1][2]. However, to date limited tests have been performed on material from the Ten Boer member, which is overlying the Rotliegendes reservoir material [3]. It is known that besides pure shale, sandy streaks are present in the Ten Boer formation.

The main aim of the present study is to characterize the behaviour of the Ten Boer material, and parameterize the data via linear elastic constants such as uniaxial compressibility, Young's modulus, Poisson's ratio and depletion constant. For this purpose, fourteen pore pressure depletion tests have been performed. Here, we document the mechanical tests conducted. Details of the sample preparation, test protocols are presented in Section 2. All test results are summarized in Section 3 and detailed triaxial test results and sample information, equipment description, photographs/scans are included in the Appendices.

2. Methods

2.1. Sample and pore fluid preparation

The Moddergat-3 core material was drilled (in June 2012) using oil-based mud and preserved in aluminium barrels directly after drilling. The core diameter is 2 5/8 inch. All 110 meter of core material was computed tomography (CT) scanned in the barrel to identify the lithology, and aiding the selection of sub-sampling locations. Samples were drilled with a length of 76 mm and a diameter of 36 mm. The vertical samples were drilled along the core axis. Due to the well inclination of 22°, plugs had to be drilled parallel to the core axis to provide sufficient length. Therefore, the plugs are not drilled perpendicular to bedding. Sample drilling was carried out using artificial brine as a cooling and lubrification fluid. The composition of the brine is given in

Table 1. The artificial brine is also used as pore fluid in all tests reported here. Sample number are in sequence of drilling.

For experiments, only intact samples or samples which did not show cracks in the CT scans were used. From the sandy streaks of the Ten Boer formation, eight samples were obtained. Six samples were drilled from pure shale material from the Ten Boer formation material. Table 2 lists the sample numbers, depth and lithology of samples used for this experimental project. Photographs and CT-scans of plugs are given in the Appendix 1.

Immediately after drilling, the sample was photographed and CT scanned. Storage of the sample was performed in artificial brine.

To avoid dry-out or possible damage to the samples, no permeability, grain density or porosity was measured.

Table 1: Composition of artifial brine

salt	Concentration [g.l^{-1}]
NaCl	205.7
KCl	4.3
$CaCl_2.2H_20$	0.1
$MgCl_2.6H_20$	19.6

Table 2: Samples, depth and lithology used for pore pressure depletion tests

Sample	Depth [m]	Lithology
6B	3777.12	Shaly sandstone
7B	3779.97	shale
18A	3786.07	Shale with thin sand laminae and lenses
20A	3801.99	Shaly sandstone
20B	3801.99	Shaly sandstone
10A	3806.27	shale
17A	3807.29	shale
17B	3807.29	shale
2A	3812.27	Shaly sandstone
2B	3812.27	Shaly sandstone
12A	3812.42	Shale with thin sand laminae
3B	3812.88	Shaly sandstone with thin irregular shale laminae
4A	3816.09	Shaly sandstone
4C	3816.09	Shaly sandstone

2.2. Experimental conditions and procedures.

To investigate the behavior of the Ten Boer claystone formation, in particular the magnitude of the strain response to stress changes, we carried out uniaxial pore pressure depletion tests using plug samples. Besides shale material, there are also sandy streaks present in the Ten Boer formation which might undergo depletion causing compaction of the specific layers. Compaction might result in material properties changes, grain cracking, pore collapse, and shear failure as possible mechanisms responsible for accommodating stress changes in the reservoir.

Pore pressure depletion tests were performed on Ten Boer core plug material using a triaxial compression apparatus (Appendix 2). All stress and pore pressure changes were imposed on the sample at a rate of 1.0 MPa/h. All tests are executed at room temperature. The stress path chosen (S_{ax}, S_{rad} and P_{pore} versus time) for the present experiments was based on in-situ stresses In-situ stress and pore pressure magnitudes, as well as the expected pore pressure at maximum depletion conditions, were provided by T. Mossop (NAM/PTU/E/Q), and are listed in Table 3.

Table 3: In-situ stress for Moddergat-3.

	Stress
Axial stress S_{ax}	80 MPa
Radial stress S_{rad}	67 MPa
Initial pore fluid pressure P_{pore}	57 MPa
Pore fluid pressure at maximum depletion	3 MPa

Each experiment was conducted using a plug sample of 76 mm length and 36 mm diameter, wrapped in two layers of gauze between the sample and the sleeve. Around the sample and in direct contact with the sample, a fine-wired metal gauze was wrapped followed by a coarse wired metal gauze. Openings are cut in the metal gauze on the position of metal pins, which are used for radial displacement measurements. The sample with gauze is placed in an elastomer sleeve and mounted in the compaction cell. Porous plates are positioned at the top and bottom of the sample.

After building in, the sample was taken to a slightly higher isostatic stress of $S_{ax} = P_{rad} = \sim 2$ MPa. Brine was flushed through the pore system and around the sample to ensure a complete saturation and removal of air.

2.2.1. Shaly sandstone samples

In the early phase of this experimental project, the exact in-situ pore pressure and maximum depletion pressure were not known. Therefore, experiments were conducted with a lower initial pore pressure and higher maximum depletion pore pressure than presented in Table 3. The samples that were characterized under these different stress conditions are samples MGT3-2A, MGT3-3B and MGT3-4A which were solely drilled from the shaly sandstone streaks.

It was anticipated that the permeability, due to the lithology and gauze, would be sufficient to perform the depletion and inflation step in single steps. The depletion and inflation cycles were followed by a consolidation period. In Figure 1, an example of this stress path is presented. In Table 4, the samples, their corresponding depth and depletion range are given which were subjected to this stress path.

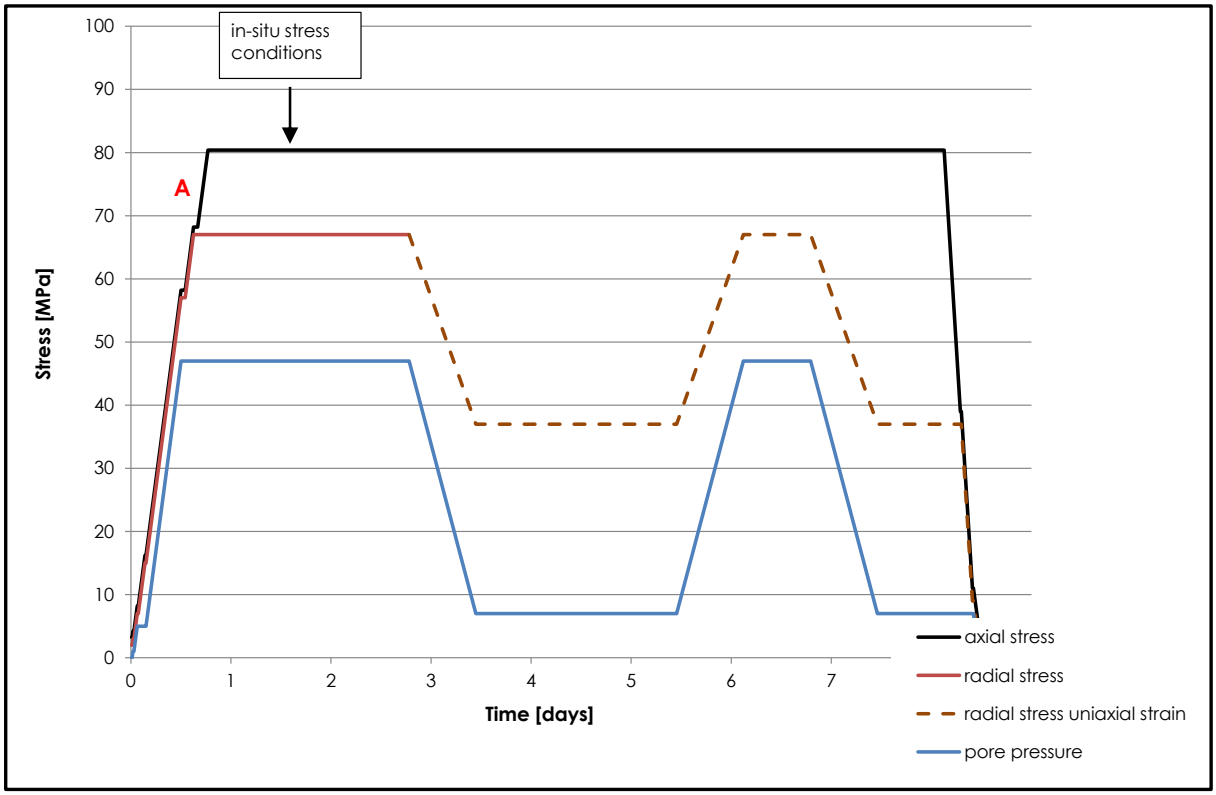

Figure 1: **Example of depletion-inflation stress path for shaly sandstone samples.**

Table 4: **Overview of test samples applying the depletion-inflation stress path and the pore pressure change during depletion.**

Sample	Depth [m]	lithology	Pore pressure change during depletion [MPa]
6B	3777.12	Shaly sandstone	57 – 3
2B	3812.27	Shaly sandstone	57 - 3
3B	3812.88	Shaly sandstone	47 – 7
4A	3816.09	Shaly sandstone	47 - 7

The stress path shown in Figure 2 was employed in the tests using shaly sandstone samples MGT3-20A and MGT3-20B with a stepwise pore pressure change from 57 MPa to 3 MPa.

2.2.2. Shale samples

The sample was taken to the in-situ stress conditions followed by equilibration of 48 hours. After the equilibration period, pore pressure depletion steps were performed under uniaxial strain conditions (i.e. zero lateral displacement) by active control of the radial total stress and under constant total vertical stress. Depletion was performed in pore pressure steps of 10 MPa, followed by an equilibration period of 48 hours with constant pore pressure. The P_{pore} depletion steps and equilibration steps were repeated until the maximum depletion pore pressure of 3 MPa was reached. An example of the stress path is shown in Figure 2.

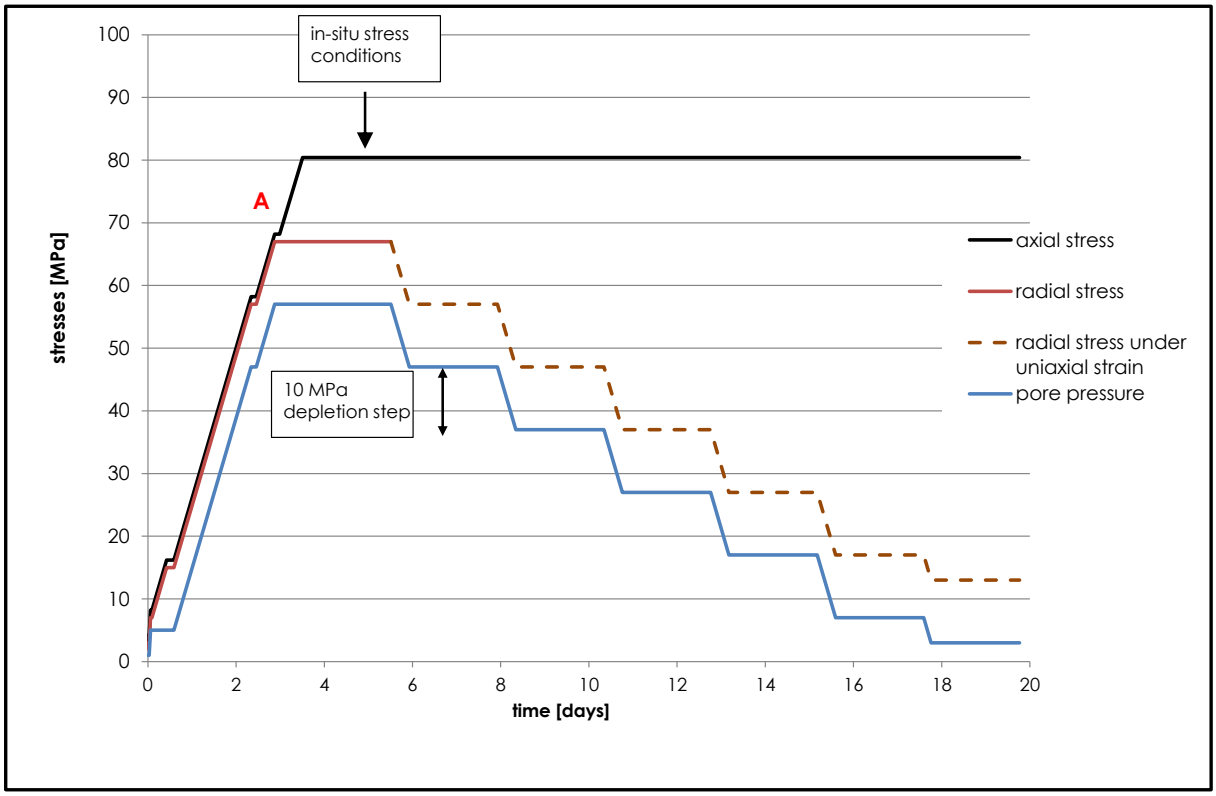

Figure 2: **Stress as a function of time for the stepwise depletion path.**

2.3. Data processing

Axial stress, radial stress and pore pressure, as well as displacements are recorded continuously. From these data, static elastic properties were determined from the slopes of stress-strain curves for each loading and unloading step (averaged over the loading/unloading time, not including the creep phase unless otherwise noted) according to linear elastic theory [4]. This included uniaxial compressibility, Young's moduli, the Poisson's ratio and the depletion constant $\gamma = \Delta\sigma_{rad}/\Delta P_{pore}$. For the calculations, no distinction is made between elastic and inelastic strains. The calculated Young's modulus and Poisson's ratio's are calculated assuming a linear elastic response to stress changes and should therefore be read as normalized strain response to stress changes.

3. Results

Five tests with shaly sandstone samples were performed using the depletion-inflation stress path presented in Figure 1. Three tests with shaly sandstone samples were performed using the stepwise depletion stress path shown in Figure 2. Table 5 presents the samples taken from the shaly sandstone streaks, the corresponding depth and the depletion range used in the pore pressure depletion tests.

Six tests with shale samples were performed using the stepwise depletion stress path shown in Figure 2 and stresses presented in Table 3.

The main trends found in the tests are:

- Higher values for Young's modulus and Poisson's ratio for shaly sandstone samples compared to pure shale samples
- No failure of the shaly sandstone samples while shear failure occurred in the shale samples.
- Stiffening of the samples in the progress of depletion.
- Plastic deformation of the samples.

Results of all individual experiments are shown in Appendix 2.

Table 5: Samples drilled from the shaly sandstone layers, their depth and depletion range.

Sample	Depth [m]	lithology	Depletion steps	Depletion range [MPa]
6B	3777.12	Shaly sandstone	single	57 – 3 [1]
20A	3801.99	Shaly sandstone	multiple	57 - 3
20B	3801.99	Shaly sandstone	multiple	57 - 3
2A	3812.27	Shaly sandstone	multiple	47 - 7
2B	3812.27	Shaly sandstone	single	57 - 3
3B	3812.88	Shaly sandstone	single	47 – 7
4A	3816.09	Shaly sandstone	single	47 - 7
4C	3816.09	Shaly sandstone	single	57 - 3

[1] during this test, oscillation of the stresses took place due to pump control problems. Only the non-oscillating parts of the test are used for data analysis.

3.1. Pore pressure depletion data shaly sandstone streaks

In all tests, the axial stress was increased from 68 MPa to 80 MPa while radial stress and pore pressure were kept constant (segment **A** in Figure 1 and Figure 2). From this axial loading step, Young's modulus and Poisson's ratio were calculated. An overview of the results is shown in Table 6.

In the test using sample MGT3-4C, a value of 5.1 GPa for the Young's modulus is obtained which is low when compared to the Young's moduli obtained with the other samples. Sample MGT3-4C is an 1 inch diameter sample and the experiment was performed without gauze around the sample. Most likely, the absence of gauze hampered the pore pressure equilibration during the test resulting in different results compared to the other tests. If the result from sample MGT3-4C is omitted, an average value for the Young's modulus of 13.2 ± 2.7 GPa is obtained.

The Poisson's ratio varied between 0.02 and 0.10 with an average value of 0.06 ± 0.03

Table 6: Young's modulus and Poisson's ratio determined in the axial loading step to in-situ axial total stress (shaly sandstone samples).

Sample ID	Depth	Young's Modulus	Poisson's ratio
	m	GPa	-
6B	3777.12	10.2	0.09
20A	3801.45	11.7	0.03
20B	3801.45	11.8	0.02
2A	3812.32	16.3	0.08
2B	3812.32	15.8	0.07
3B	3812.93	17.1	0.07
4A	3816.14	12.3	0.10
4C	3816.14	5.2	0.05
average		**12.6**	**0.06**
stdev		**3.9**	**0.03**

Samples MGT3-20A and MGT3-20B were subjected to pore pressure depletion steps of 10 MPa employed at a rate of 2.5 MPa/hr. In Table 8, an overview of the results is presented.

With sample MGT3-20A and MGT3-20B, stiffening of the samples was found in the first two depletion steps from P_{pore} = 57 MPa to 47 MPa and P_{pore} = 47 MPa to 37 MPa, respectively. The apparent Young's modulus increased from 16.5 GPa to ~28 GPa and further to ~35 GPa. In the two following depletion steps from 37 to 27 MPa and 27 to 17 MPa, the Young's modulus remained similar. The Poisson's ratio showed a constant value of 0.07 ± 0.01. A depletion constant γ of 0.88 ± 0.01 was computed on the basis of the total radial stress and pore pressure changes during the first four depletion steps.

During the depletion step from 7 MPa to 3 MPa, significant changes took place. The Young's moduli from MGT3-20A and MGT3-20B increased to 42.5 GPa and 54.4 GPa respectively. The Poisson's ratio increased while the depletion constant decreased.

Sample MGT3-2A is depleted from an initial pore pressure of 47 MPa to 7 MPa in four steps of 10 MPa. During the depletion steps, the Young's modulus gradually decreased from 22.6 GPa to 12.0 GPa indicating weakening of the sample. The values for the Poisson's ratio and depletion constant remained the same. No failure of the sample is observed as can be seen in the CT scan of the post-test sample (Figure 3). The last depletion step from 17 to 7 MPa was performed in a faster loading rate compared to the other tests due to equipment problems. No hold period at 7 MPa was carried.

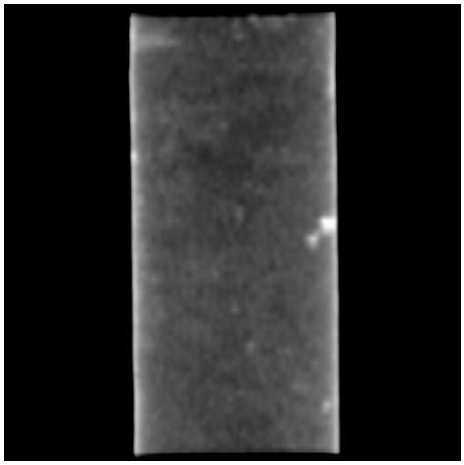

Figure 3: CT scan of post-test sample MGT3-2A.

After executing four depletion steps to 7 MPa, the pore pressure was brought back under uniaxial strain conditions to the original value of 47 MPa. The inflation from 7 to 47 MPa was done in a single step. The sample was considerable stiffer during this pore pressure inflation step and a Young's modulus of 35.4 GPa was found. The Poisson's ratio increased to a value of 0.23. These findings can be attributed to non-recoverable deformation (plastic deformation) of the sample in the pore pressure depletion step. Approximately 40% of the axial strain is recoverable during this stage of the experiment. The second uniaxial pore pressure depletion step from 47 to 7 MPa resulted in a Young's modulus of 31.1 GPa and a Poisson's ratio of 0.22.

Samples MGT3-2B, MGT3-3B, MGT3-4A, MGT3-4B and MGT3-6B were characterized applying the depletion-inflation stress path as shown in Figure 1 and pore pressure data presented in Table 4. In Table 9, an overview of the test results is presented.

The average Young's modulus varied between 8.1 GPa and 23.3 GPa with an average value of 17.5 ± 6.3 GPa. The difference between twin samples sample MGT3-4A and MGT-4C were caused by the absence of gauze in the test with sample MGT-4C which might result in pore pressure equilibration difficulties.

An average Poisson's ratio of 0.10 ± 0.04 and an average depletion constant 0.88 ± 0.04 was calculated.

The found elastic parameters found in these five tests are in line with the parameters found with MGT3-20A and MGT3-20B (compared to first 10 MPa depletion) and sample MGT3-2A.

After a consolidation period at anticipated maximum depletion conditions, the pore pressure was taken back to the original in-situ value under uniaxial strain conditions which was done in a single step. Considerable increases in Young's moduli were found (27.7 ± 6.9 GPa). The average value of the Poisson's ratio increased to 0.15 ± 0.03. The increase in Young's moduli and Poisson's ratio are caused by plastic deformation of the samples resulting in sample stiffening. During the inflation step, 64-73% of the axial strain accumulated during the pore pressure depletion step was recovered (i.e. elastic strain) during the pore pressure inflations step.

For the second pore pressure depletion cycle, similar elastic parameters were found.

In comparison, similar Young's moduli, Poisson's ratio and depletion constant γ were found for samples from the shaly sandstone layers from the Ten Boer formation. An overview of the average Young's modulus, Poisson's ratio and depletion constant are presented in Table 7. In this

overview, the results from sample MGT3-4C are omitted. The values are obtained from the first depletion step and first 10 MPa depletion of samples MGT3-20A and MGT3-20B.

In all tests, the samples remained intact and no shear failure of the samples was observed.

Table 7: Average Young's modulus, Poisson's ratio and depletion constant of the shaly sandstone tests determined in the first depletion step.

	Young's modulus	Poisson's ratio	Depletion constant γ
	[GPa]	[-]	[-]
average	19.9 ± 3.9	0.09 ± 0.03	0.88 ± 0.03

Table 8: **Results of the pore pressure depletion tests with shaly sandstone samples from the Ten Boer formation applying the stepwise depletion stress path (Figure 2).**

depletion		57 - 47 MPa			47 - 37 MPa			37 - 27 MPa			27 - 17 MPa			17 - 7 MPa			7 - 3 MPa		
Sample ID	Depth	Young's Modulus	Poisson's ratio	Depletion constant	Young's Modulus	Poisson's ratio	Depletion constant	Young's Modulus	Poisson's ratio	Depletion constant	Young's Modulus	Poisson's ratio	Depletion constant	Young's Modulus	Poisson's ratio	Depletion constant	Young's Modulus	Poisson's ratio	Depletion constant
	m	GPa	-	-	GPa	-	-	GPa	-	-	GPa	-	-	GPa	-	-	GPa	-	-
20A	3801.45	17.2	0.09	0.87	26.6	0.08	0.88	36.9	0.07	0.88	34.9	0.07	0.87	37.3	0.09	0.85	43.9	0.19	0.70
20B	3801.45	17.0	0.07	0.90	29.7	0.06	0.90	34.2	0.06	0.9	37.1	0.06	0.89	33.2	0.06	0.89	56.0	0.09	0.83
2A	3812.32	-	-	-	22.6	0.11	0.87	20.2	0.12	0.86	15.2	0.10	0.87	12	0.11	0.87	-	-	-

Table 9: **Results of the pore pressure depletion tests with shaly sandstone samples from the Ten Boer formation applying the pore pressure depletion-inflation stress path (Figure 1).**

		1st pore pressure depletion step			pore pressure inflation step			2nd pore pressure depletion step		
Sample ID	Depth	Young's Modulus	Poisson's ratio	Depletion constant γ	Young's Modulus	Poisson's ratio	Depletion constant γ	Young's Modulus	Poisson's ratio	Depletion constant γ
	m	GPa	-	-	GPa	-	-	GPa	-	-
2B	3812.32	23.3	0.09	0.90	31.6	0.15	0.82	29.6	0.16	0.81
3B	3812.93	22.9	0.05	0.95	32.1	0.12	0.85	30.9	0.12	0.85
4A	3816.14	15.2	0.07	0.90	29.7	0.14	0.80	27.2	0.14	0.79
4C	3816.14	8.1	0.16	0.81	17.4	0.20	0.76	15.4	0.20	0.75
6B	3777.12	18.1	0.13	0.83	-	-	-	-	-	-
average		17.5	0.10	0.88	27.7	0.15	0.81	25.8	0.14	0.80
stdev		6.3	0.04	0.06	6.9	0.03	0.04	7.1	0.02	0.04
average	(4C excluded)	19.9	0.09	0.90	31.1	0.14	0.82	29.2	0.14	0.82
stdev		3.9	0.03	0.05	1.3	0.02	0.03	1.9	0.02	0.03

3.2. Tests with samples from shale material

In all tests, the axial stress was increased from 68 MPa to 80 MPa while radial stress and pore pressure were kept constant (displayed as segment A in Figure 2). From this axial loading step, Young's modulus and Poisson's ratio were calculated. An overview of the results is given in Table 10. The average value for the Young's modulus determined in this axial loading step amounts to 8.9 ± 1.7 GPa.

Low values for the Poisson's ratio were found in three experiments. In tests with samples MGT3-17A, -17B and 12A, the Poisson's ratio was negative. In all probability, this is caused by the low permeability of the shale samples resulting in a non-uniform pore pressure distribution or delayed pore pressure response in the sample.

Table 10: Young's modulus and Poisson's ratio determined in the axial loading step to in-situ axial total stress (shale samples).

Sample ID	Depth	Young's Modulus	Poisson's ratio
	m	GPa	-
7B	3779.97	8.7	0.01
18A	3786.07	11.6	0.02
10A	3806.27	8.4	0.02
17A	3807.29	10.0	-
17B	3807.29	8.1	-
12A	3812.42	6.6	-
average		**8.9**	**0.02**
stdev		**1.7**	**0.01**

The results of the pore pressure depletion steps with shale samples are summarized in Table 11.

In the first depletion step from P_{pore} = 57 MPa to 47 MPa, Young's moduli varied between 10.4 GPa and 15.2 GPa with an average value of 12.8 ± 1.7 GPa. Low values for the Poisson's ratio were found with values of less than 0.07 (average value: 0.04 ± 0.03). The depletion constant γ varied between 0.90 and 1.00 with an average value of 0.95 ± 0.04.

For all samples, stiffening was observed in the second depletion step from P_{pore} = 47 MPa to 37 MPa. Young's moduli varied between 12.1 GPa and 19.4 GPa with an average value of 14.6 ± 2.7 GPa. The Poisson's ratio increased to an average value of 0.07 ± 0.02 and γ decreased to 0.90 ± 0.03.

In the third depletion step (P_{pore}: 37 – 27 MPa), a mixed behaviour was found. Sample MGT3-10A, MGT3-17A and MGT3-18A showed stiffening resulting in higher Young's moduli. Samples MGT3-7B and -17B showed weakening resulting in lower Young's moduli. In both cases, an increase of the Poisson's ratio and decrease of the depletion constant was found.

Sample MGT3-12A showed failure indicated by a significant increase in axial strain and radial stress. The failure resulted in a decrease in Young's modulus from 11.8 GPa to 6.4 GPa while the depletion constant γ showed a drop from 0.93 to 0.63.

In the fourth depletion step (P_{pore}: 27 – 17 MPa), failure of sample MGT3-7B took place indicated by an increase in axial strain and radial stress.

The already failed sample MGT3-12A showed stiffening in this depletion step (P_{pore}: 27 – 17 MPa) which resulted in an increased Young's modulus (9.6 GPa). The Poisson's ratio and depletion constant remained similar, 0.24 and 0.62 respectively.

The intact samples showed all weakening with a slight reduction of the Young's modulus.

The tests with samples MGT3-10A and MGT3-17A were stopped at a pore pressure of 17 MPa due to equipment problems. However, the reduction of depletion constant γ observed in both tests might indicate starting of sample failure.

In the fifth depletion step (P_{pore}: 17 – 7 MPa), failure of sample MGT3-17B was observed exhibiting the same trend with respect to axial strain and radial stress as seen in the other shear failures. In Figure 4, the stress-strain curve of pore pressure depletion step for sample MGT3-17B is shown. In Figure 5, the post-test CT scan of sample MGT3-17B is shown. The scan showed a clear shear failure as a result of the increased differential stress ($S_{ax} – S_{rad}$).

A continuous weakening of sample MGT-3-7B was observed with a decrease of the Young's modulus to 1.6 GPa and a simultaneous increase of the radial stress to compensate for radial expansion of the sample.

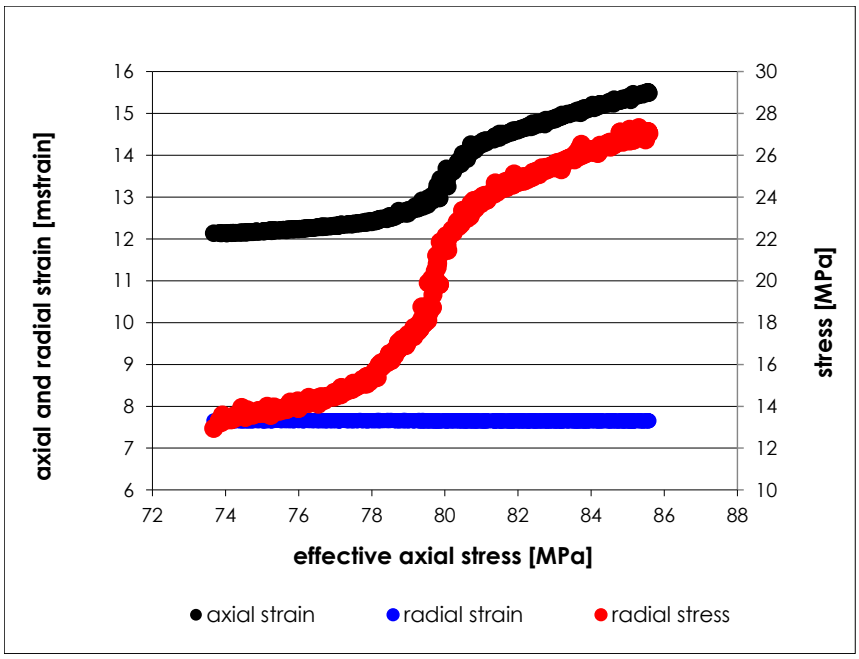

Figure 4: Sample MGT3-17B: stress-strain curve for pore pressure depletion step (P_{pore}: 17 MPa to 7 MPa).

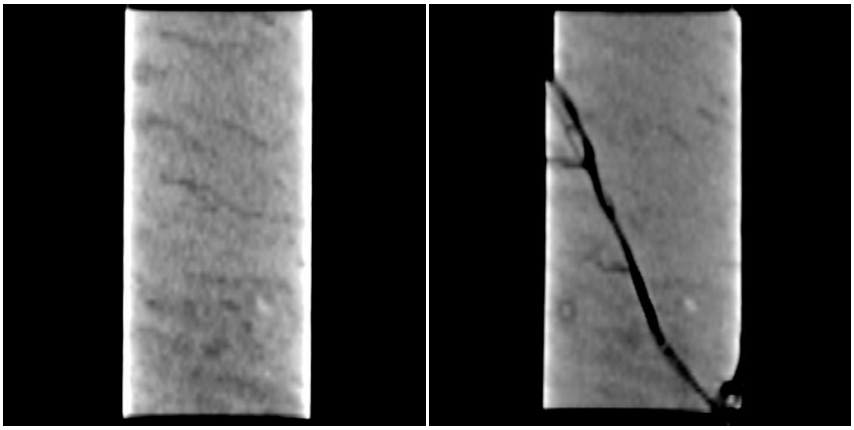

Figure 5: Sample MGT3-17B: CT scan of pre-test (left) and post-test (right) sample.

In the last depletion step (P_{pore}: 7- 3 MPa), all samples became stiffer indicated by higher values of the Young's modulus. The Poisson's ratio increased as well.

The only sample that remained intact during the whole test was sample MGT3-18A. The trend of sample stiffening and weakening during the pore pressure depletion steps with this sample was similar as observed in the other depletion experiments with shale samples.

Sample MGT3-18A was subjected to a stepwise pore pressure inflation step from maximum depletion pore pressure to the original in-situ pore pressure under uniaxial strain conditions. Each pore pressure step was 10 MPa and was followed by an equilibration period of 48 hours. The Young's modulus determined during the first inflation step (P_{pore} = 3 MPa to 7 MPa) was 26.2 GPa while in the same pore pressure range during the depletion step, a Young's modulus of 18.6 GPa was found. In the subsequent pore pressure inflation steps of 10 MPa, the Young's moduli and Poisson's ratio's were higher than determined in the corresponding pore pressure depletion steps. This indicates a stiffer sample due to non-recoverable deformation.

In Figure 6 and Figure 7, the evolution of the Young's modulus and depletion constant γ for the individual pure shale samples during the six depletion steps are shown. Figure 8 shows the Young's modulus from the first (P_{pore}: 57 – 47 MPa) and second pore pressure depletion steps (P_{pore}: 47 – 37 MPa) plotted versus the sample depth for the Ten Boer shale samples.

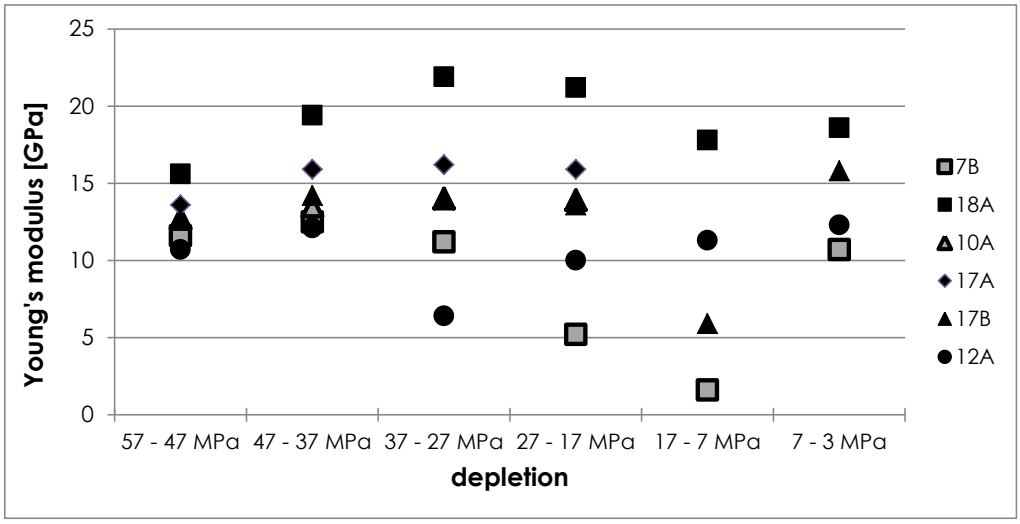

Figure 6: **Evolution of the Young's modulus parameterized from measured stress-strain response during the pore pressure depletion steps for the Ten Boer shale samples.**

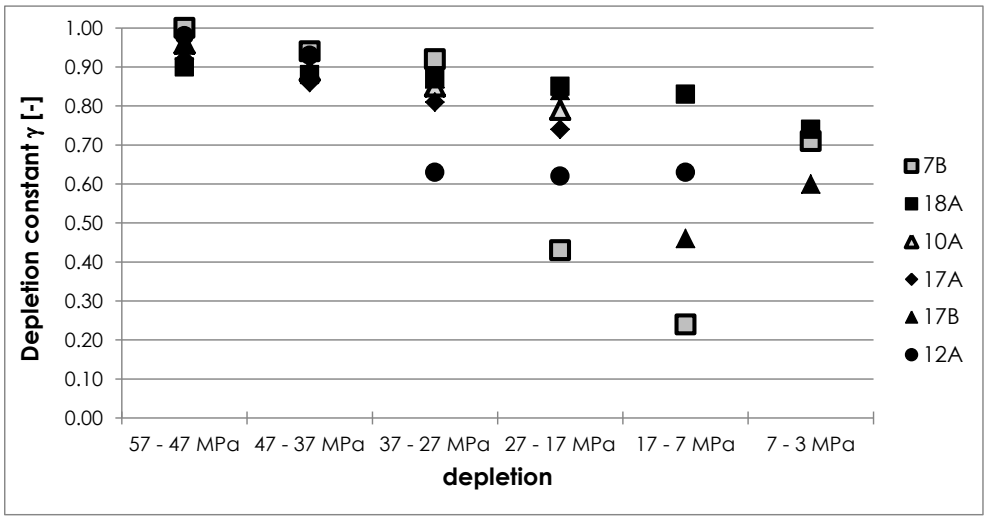

Figure 7: **Depletion constant parameterized on the basis of the change in radial stress and pore pressure measured during depletion for all samples, and plotted versus pore pressure depletion change.**

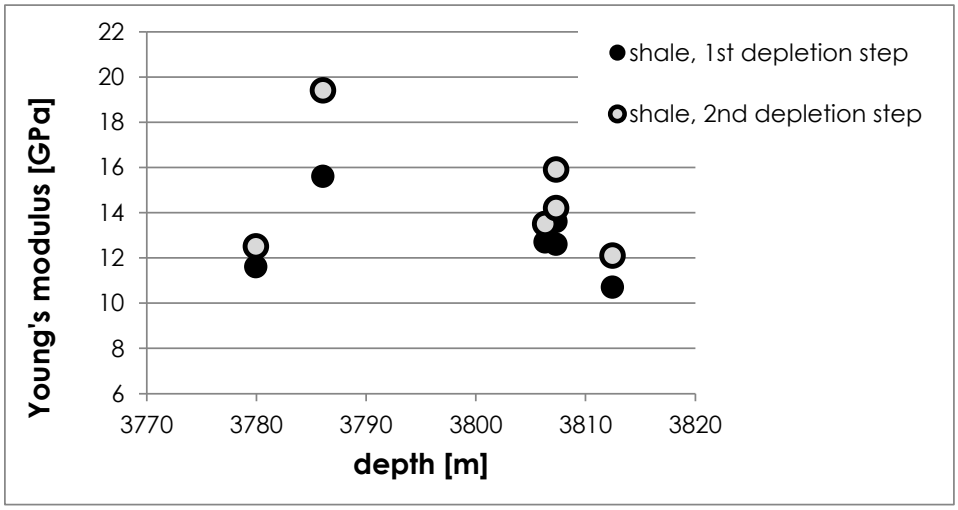

Figure 8: **The Young's modulus, parameterized from measured stress-strain response, plotted versus sample depth of the Ten Boer shale samples. The Young's modulus were determined during for the first (P_{pore} = 57 MPa to 47 MPa) and second (P_{pore} = 47 to 37 MPa) pore pressure depletion step.**

Table 11: Results of the pore pressure depletion experiments with shale samples from the Ten Boer formation.

depletion		57 - 47 MPa			47 - 37 MPa			37 - 27 MPa			27 - 17 MPa			17 - 7 MPa			7 - 3 MPa		
Sample ID	Depth	Young's Modulus	Poisson's ratio	Depletion constant	Young's Modulus	Poisson's ratio	Depletion constant	Young's Modulus	Poisson's ratio	Depletion constant	Young's Modulus	Poisson's ratio	Depletion constant	Young's Modulus	Poisson's ratio	Depletion constant	Young's Modulus	Poisson's ratio	Depletion constant
	m	GPa	-	-	GPa	-	-	GPa	-	-	GPa	-	-	GPa	-	-	GPa	-	-
7B	3779.97	11.6	-	1.00	12.5	0.04	0.94	11.2	0.06	0.92	5.2	0.35	0.43	1.6	0.40	0.24	10.7	0.21	0.71
18A	3786.07	15.6	0.07	0.90	19.4	0.08	0.88	21.9	0.09	0.87	21.2	0.10	0.85	17.8	0.12	0.83	18.6	0.17	0.74
10A	3806.27	12.7	0.02	0.96	13.5	0.08	0.89	14	0.11	0.85	13.9	0.15	0.79						
17A	3807.29	13.6	0.06	0.92	15.9	0.1	0.86	16.2	0.13	0.81	15.9	0.18	0.74						
17B	3807.29	12.6	0.03	0.96	14.2	0.08	0.89	14	0.09	0.87	13.6	0.12	0.84	*5.9*	*0.37*	*0.46*	15.8	0.25	0.6
12A	3812.42	10.7	0.01	0.98	12.1	0.05	0.93	6.4	0.24	0.63	10	0.24	0.62	11.3	0.24	0.63	12.3	0.2	0.70
average		**12.8**	**0.04**	**0.95**	**14.6**	**0.07**	**0.90**												
stdev		**1.7**	**0.03**	**0.04**	**2.7**	**0.02**	**0.03**												

Note: the pink colored cells indicate failure of the sample.

4. Summary of key observations

We have characterized the mechanical response of Ten Boer cap rock material, taken from well Moddergat-3 (Nes gas field, The Netherlands), by subjecting it to pore pressure depletion and inflation under uniaxial strain boundary conditions. Experiments have been conducted on 14 plugs sub-sampled from the core, of which 8 were shaly sandstone, and 6 shale samples. All stress-strain data have been parameterized by applying linear elastic theory, to obtain the uniaxial compressibility Cm, Young's modulus E, Poisson's ratio υ and depletion constant γ. We here summarize our key findings.

During the first pore pressure depletion cycle, the stiffness of shales, expressed here in terms of the Young's Modulus and Poisson's ratio, is distinctly lower compared to shaly sandstones. However, shale samples exhibit strong stiffening during the first depletion step from Ppore = 57 MPa to 47 MPa, which suggests a consolidation mechanism to operate initially in these samples.

Progressive weakening and failure occurred in most shale samples during pore pressure depletion. One exception was shale sample MGT3-18A (depth: 3786.07 m), that remained intact, but transitioned from stiffening to weakening behaviour. By contrast, no shear failure occurred in the shaly sandstone samples.

Comparing now recoverable and non-recoverable strains during first depletion versus inflation shows that 64-73% of the axial strain in the shaly sandstone was recoverable. For the case of shale sample MGT3-18A, roughly 65% of the attained strain was recoverable. These observations confirm the stiffening response observed, and suggest that the magnitude of the first consolidation (i.e. ⅓ inelastic strain), for those samples that did not yield, is independent of lithology.

As the Ten Boer member consists of an interbedded sequence of shale and thin streaks of shaly sandstone, it is expected that the mechanical behavior is controlled by the shale mass. The observed shear failure might be considered a concern that deserves attention in future research. However, note that the applicability of the stress path employed in this study for reservoir simulations depends on whether pore pressure equilibration is feasible. Permeability measurements on a number of selected samples from this interval suggest that this is challenging, although our data provide no evidence for major delayed poroelastic effects.

References

[1] EP 2010-5359, "Creep in Groningen Sandstone", A.D. Post, J.W. Dudley, P.A. Fokker, A.J. van der Linden

[2] EP 2000-5646, "The compressibility of Groningen reservoir sandstone - Experimental research by SIEP-RTS, from 1990 - 1995", P.M.T.M. Schutjens, J.W. Beljaars, P.A.G. van der Geest, M. Hettema, H. de Ruig, H. Visser, J.Y. Essiane Essone

[3] RKTR.87.310, "Compaction and permeability study on the Ten Boer claystone samples from the Groningen field, The Netherlands", R. Vlaardingerbroek.

[4] Petroleum Related Rock Mechanics, E. Fjaer, R.M. Holt, P. Horsrud, A.M. Raaen and R. Risnes, 2nd edition published 2008.

Appendix 1. Photographs and CT scans of Ten Boer samples.

A1.1 Photographs of pre-test and post-test samples.

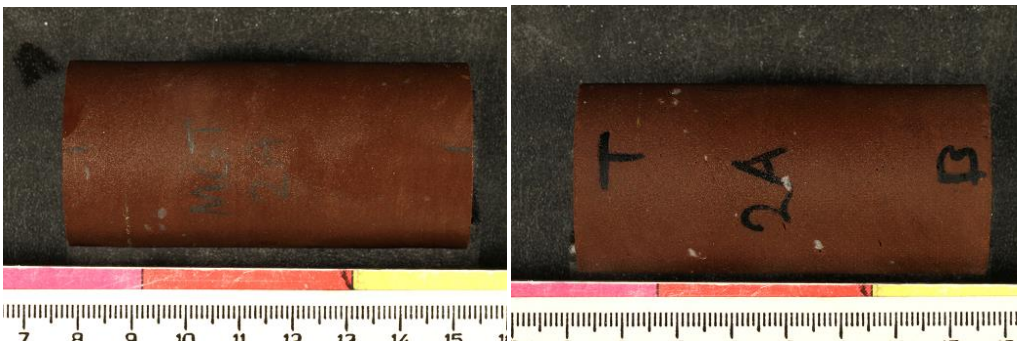

Figure A1.1: photograph sample MGT3-2A (pre-test: left, post-test: right)

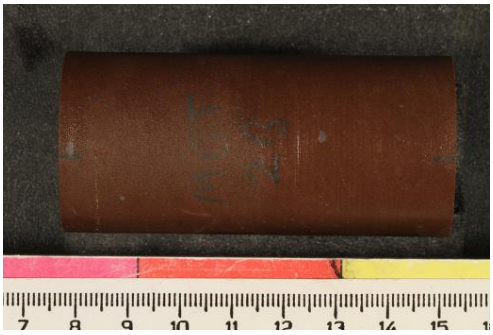

Figure A1.2: photograph sample MGT3-2B (pre-test only)

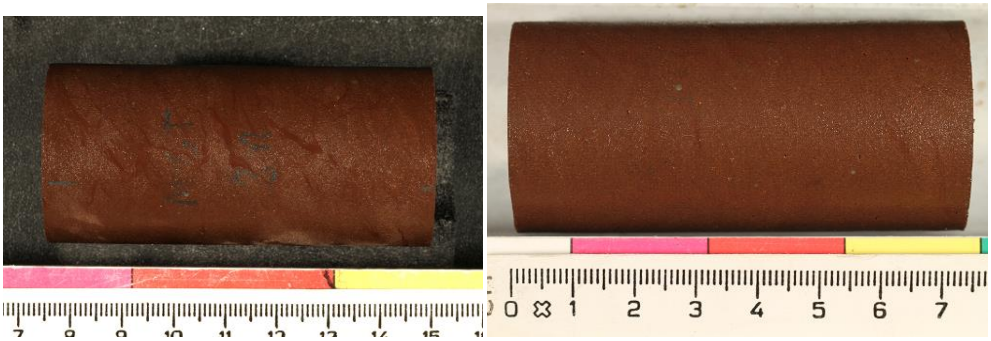

Figure A1.3: photograph sample MGT3-3B (pre-test: left, post-test: right)

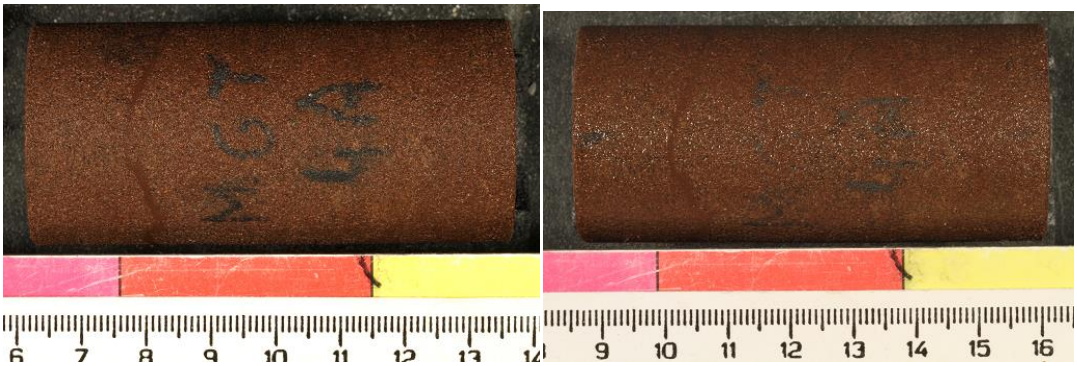

Figure A1.4: Photograph of sample MGT3-4A (pre-test: left, post-test: right)

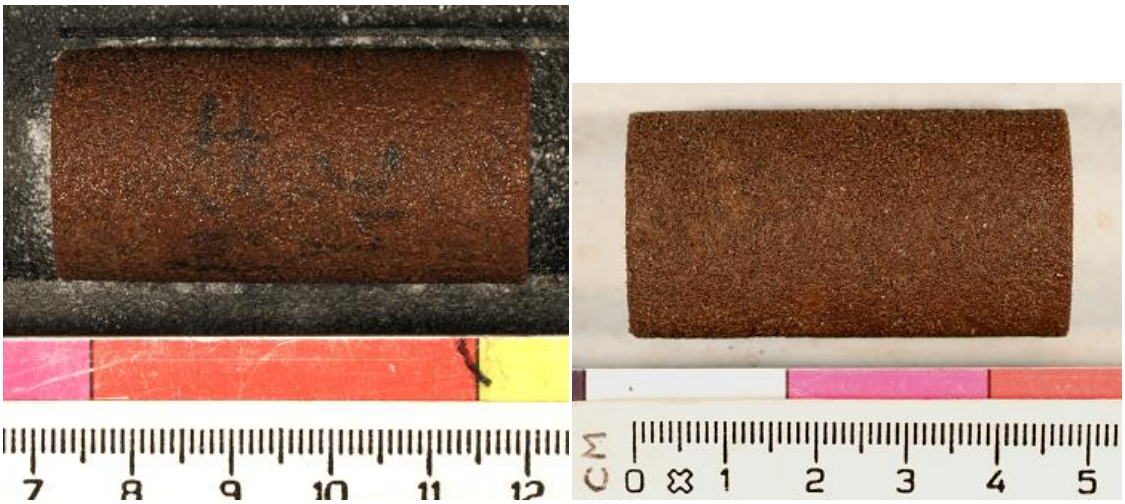

Figure A1.5: Photograph of sample MGT3-4C (pre-test: left, post-test: right)

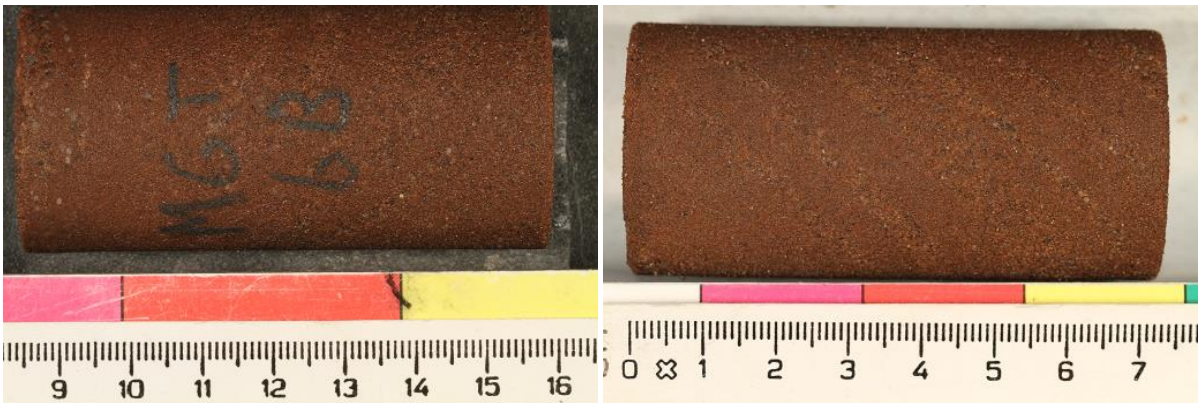

Figure A1.6: Photograph of sample MGT3-6B (pre-test: left, post-test: right)

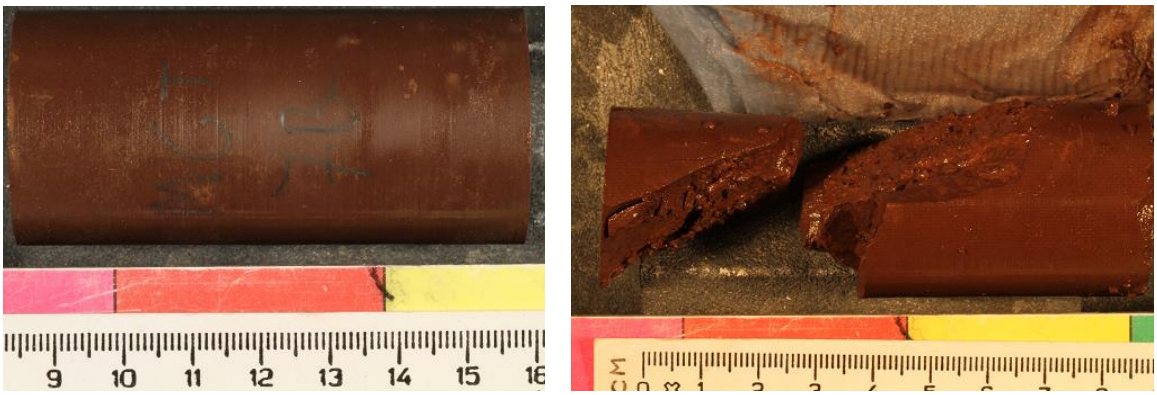

Figure A1.7: Photograph of sample MGT3-7B (pre-test: left, post-test: right)

Figure A1.8: Photograph of sample MGT3-10A (pre-test: left, post-test: right)

Figure A1.9: Photograph of sample MGT3-12A (pre-test: left, post-test: right)

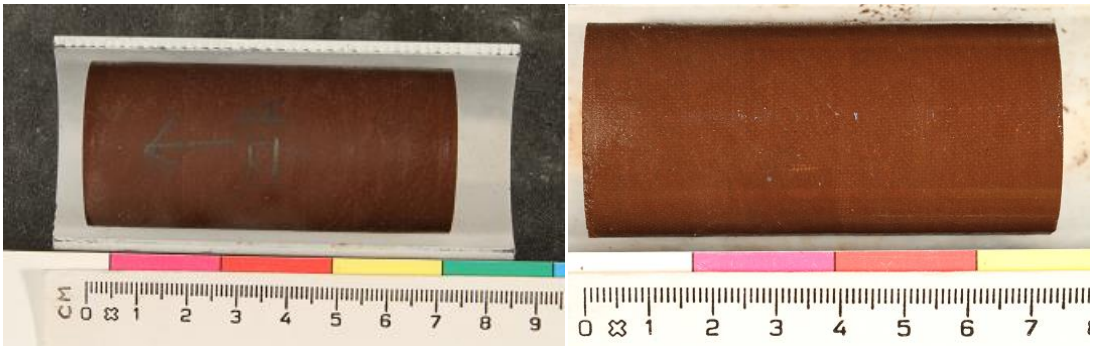

Figure A1.10: Photograph of sample MGT3-17A (pre-test: left, post-test: right)

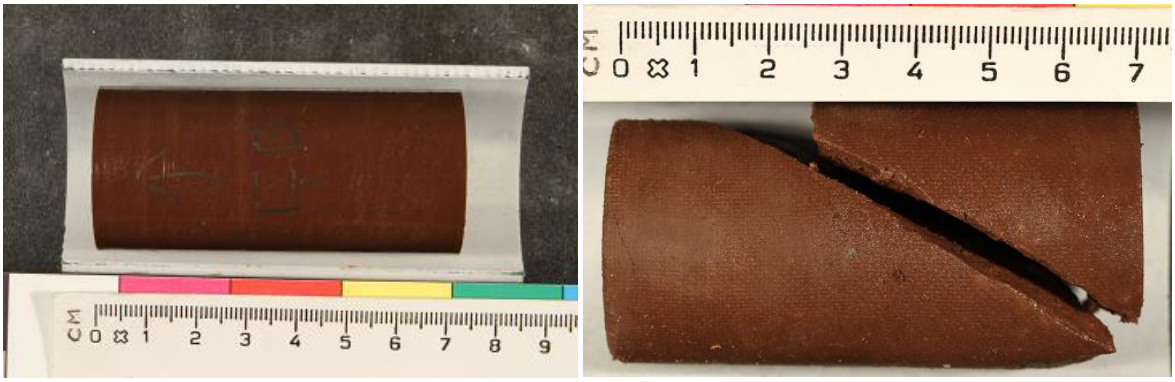

Figure A1.11: Photograph of sample MGT3-17B (pre-test: left, post-test: right)

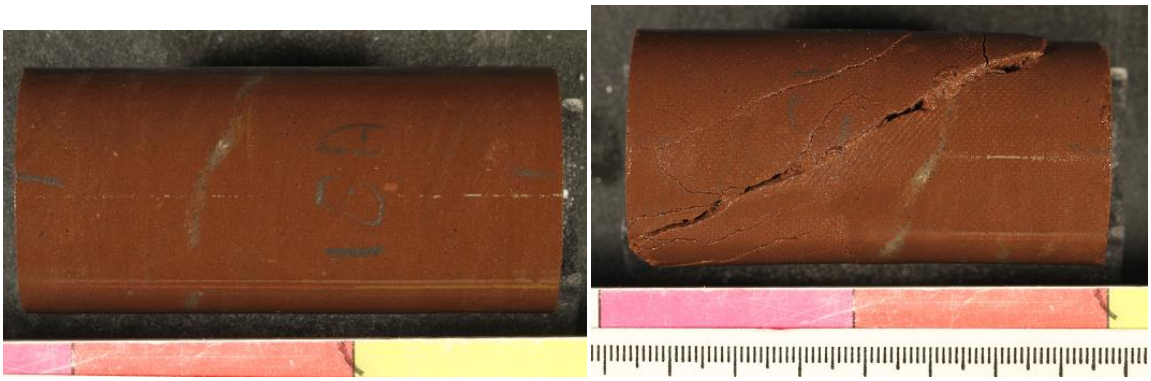

Figure A1.12: Photograph of sample MGT3-18A (pre-test: left, post-test: right)

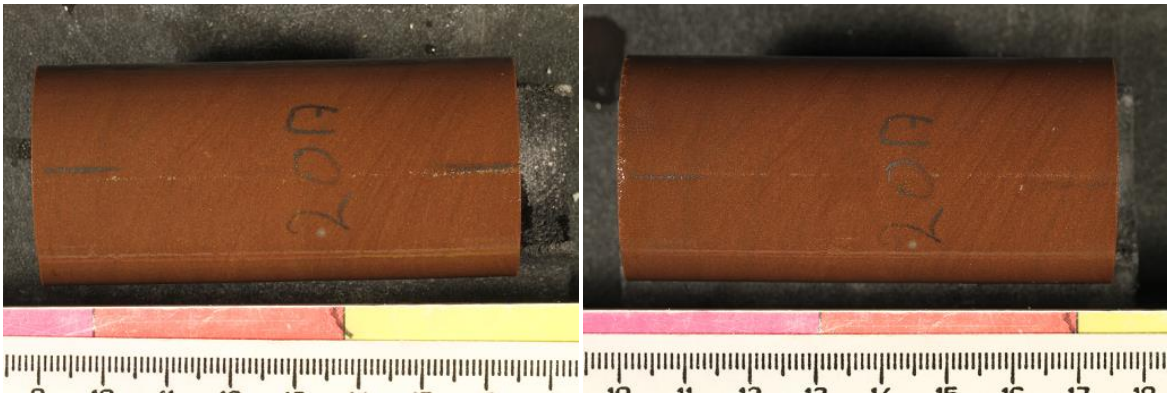

Figure A1.13: Photograph of sample MGT3-20A (pre-test: left, post-test: right)

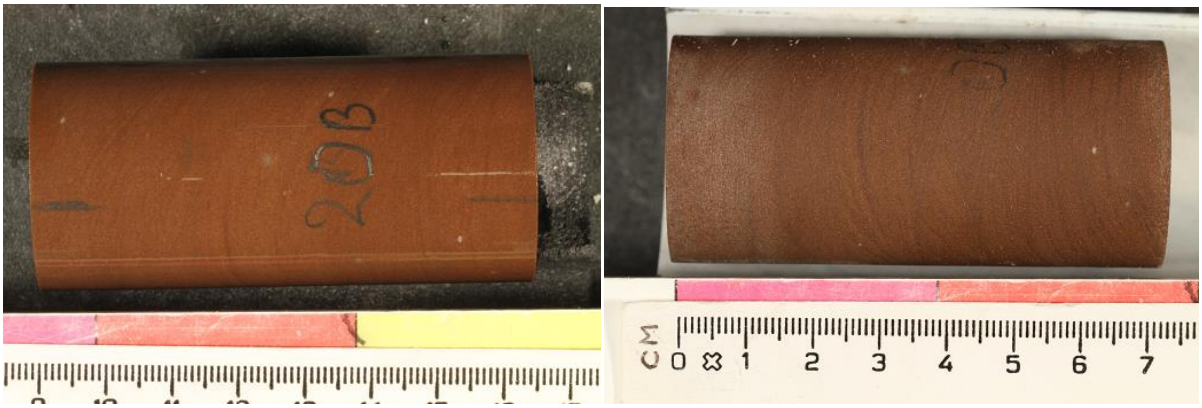

Figure A1.14: Photograph of sample MGT3-20B (pre-test: left, post-test: right)

A1.2 CT scans of pre-test and post-test samples.

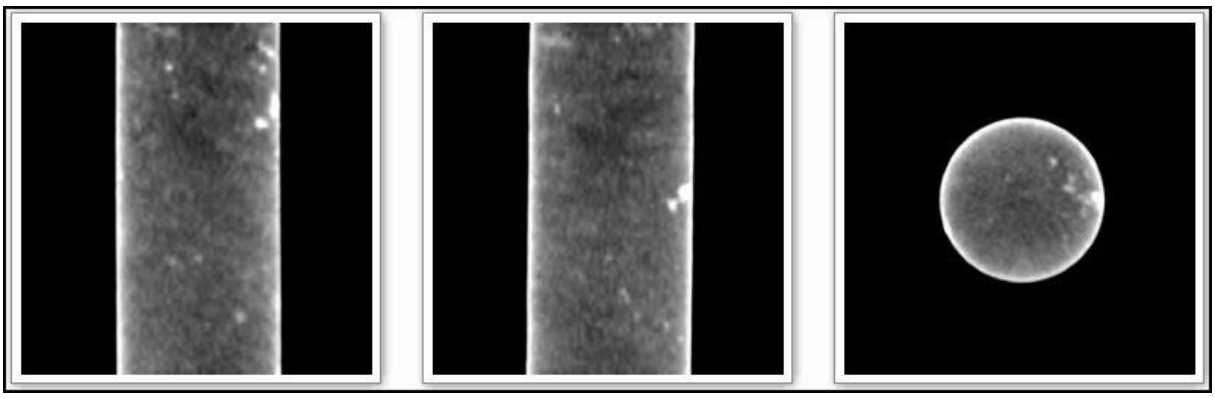

Figure A1.15: CT scans of pre-test samples MGT3-2A

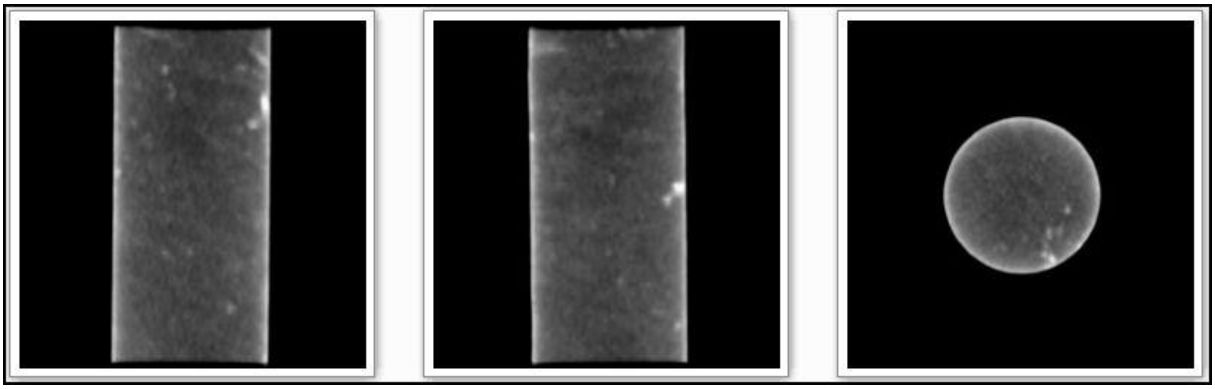

Figure A1.16: CT scans of post-test samples MGT3-2A

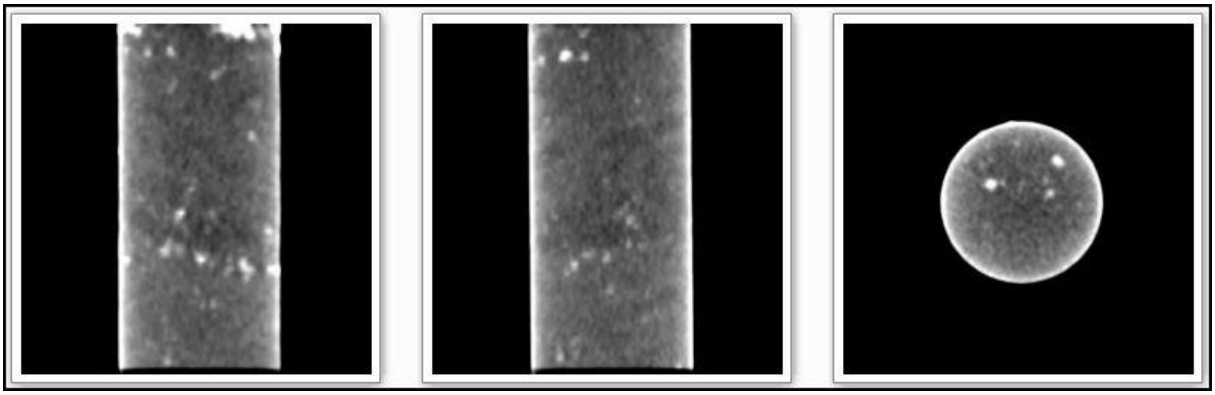

Figure A1.17: CT scans of pre-test samples MGT3-2B

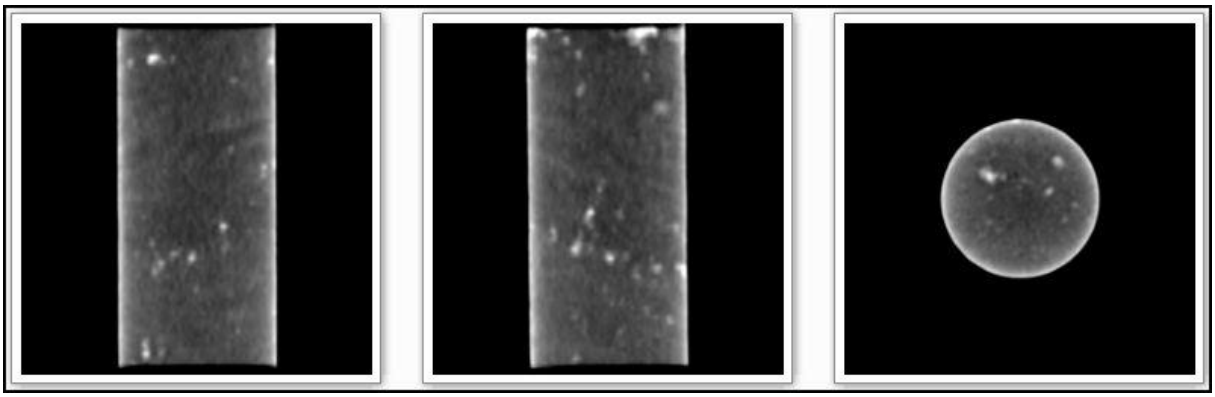

Figure A1.18: CT scans of post-test samples MGT3-2B

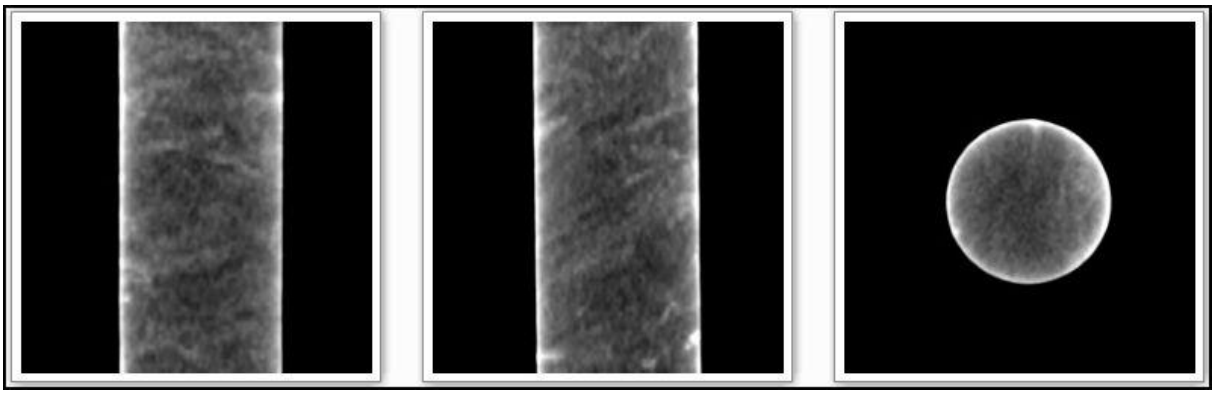

Figure A1.19: CT scans of pre-test samples MGT3-3B

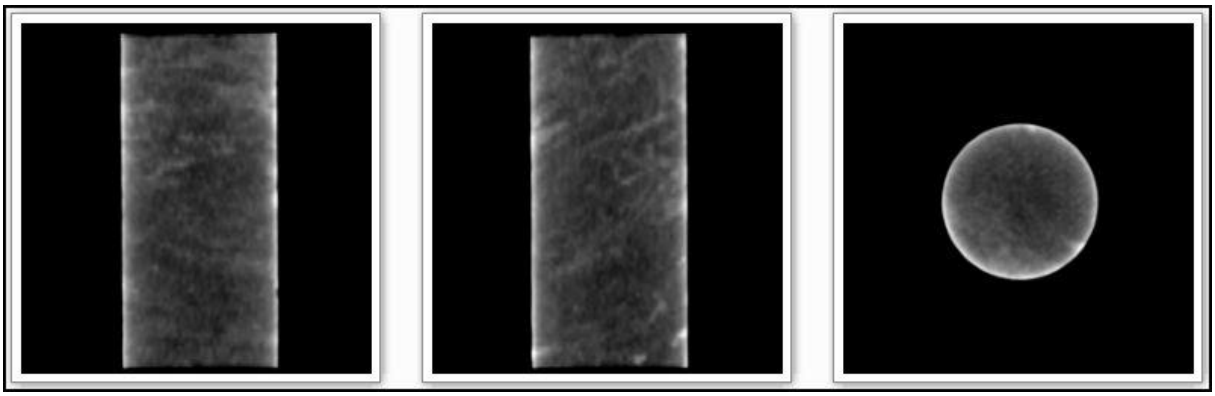

Figure A1.20: CT scans of post-test samples MGT3-3B

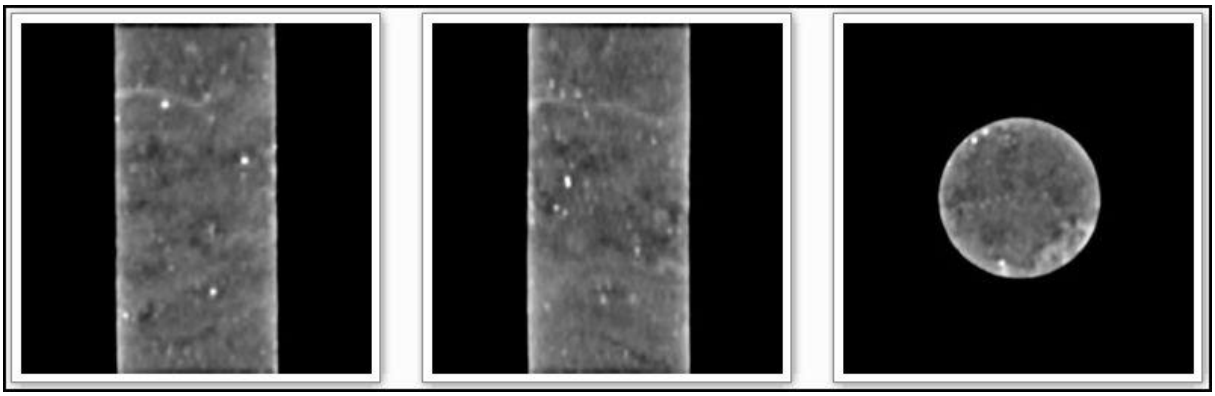

Figure A1.21: CT scans of pre-test samples MGT3-4A

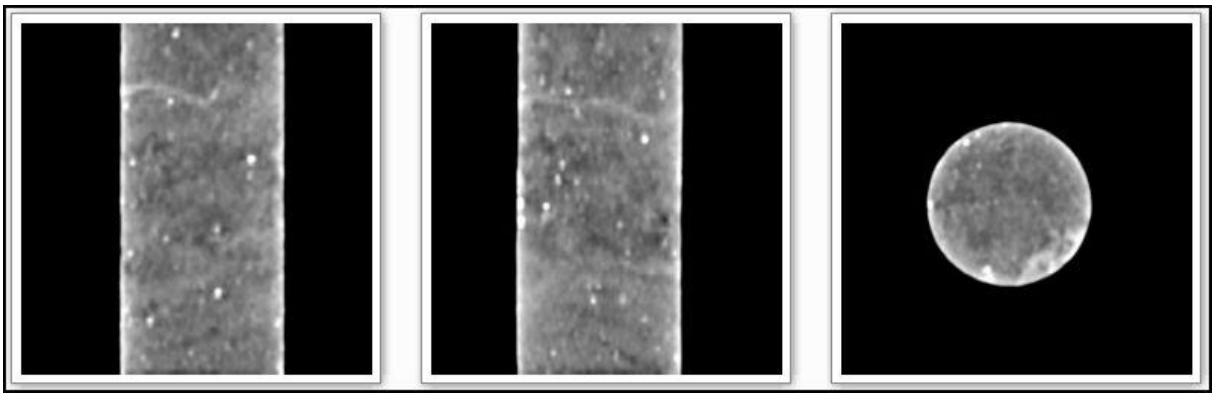

Figure A1.22: CT scans of post-test samples MGT3-4A

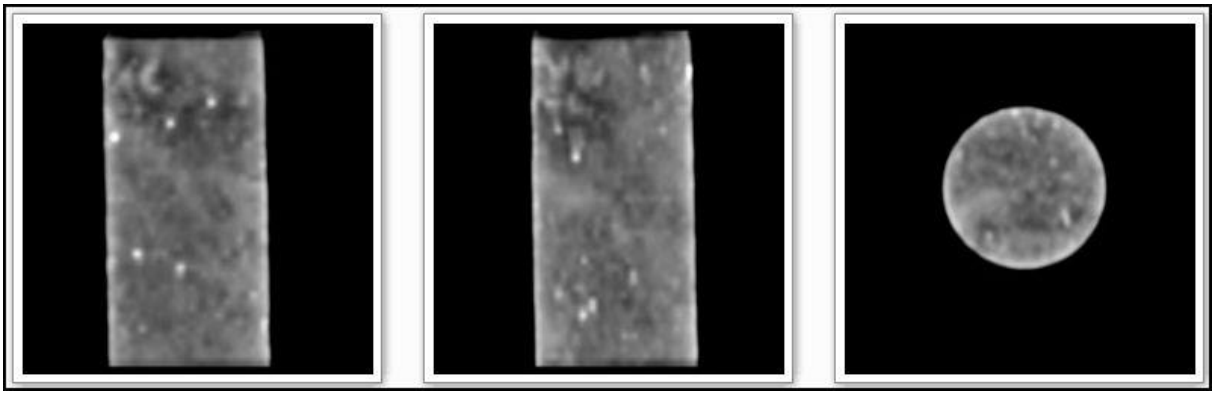

Figure A1.23: CT scans of pre-test samples MGT3-4C

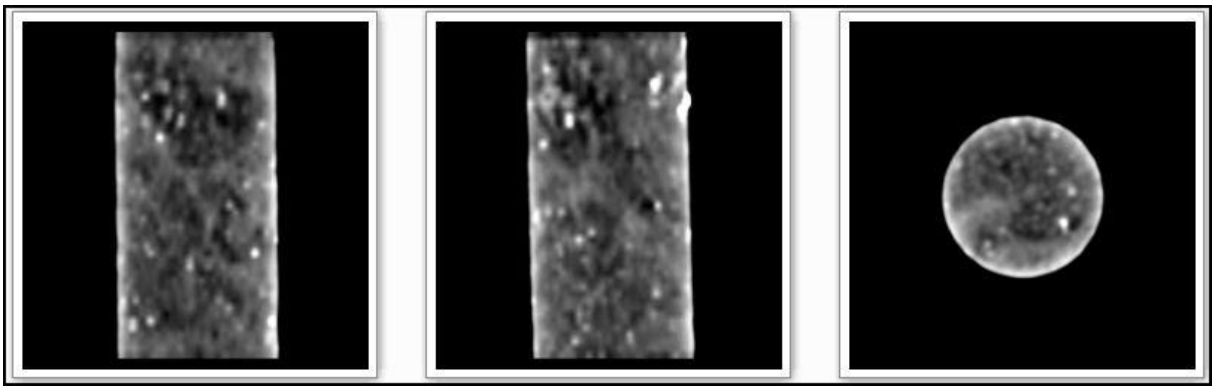

Figure A1.24: CT scans of post-test samples MGT3-4C

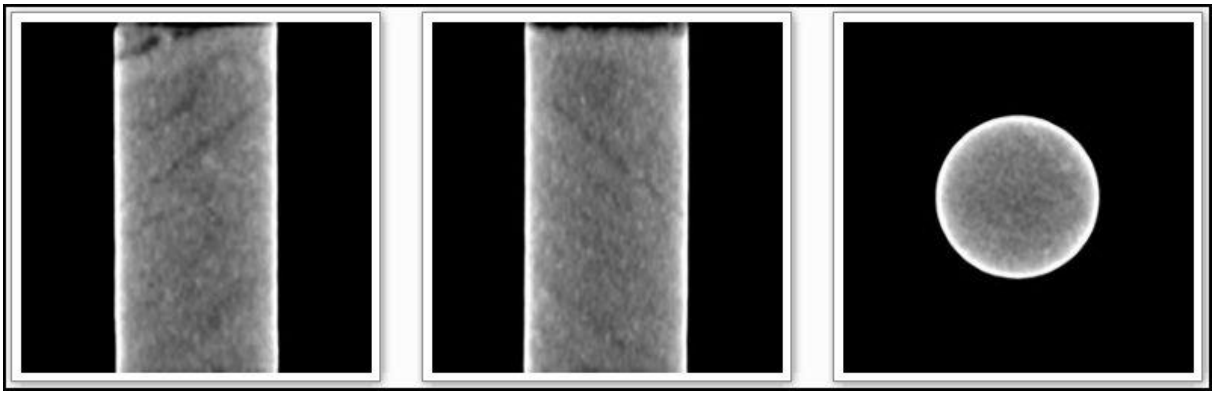

Figure A1.25: CT scans of pre-test sample MGT3-6B

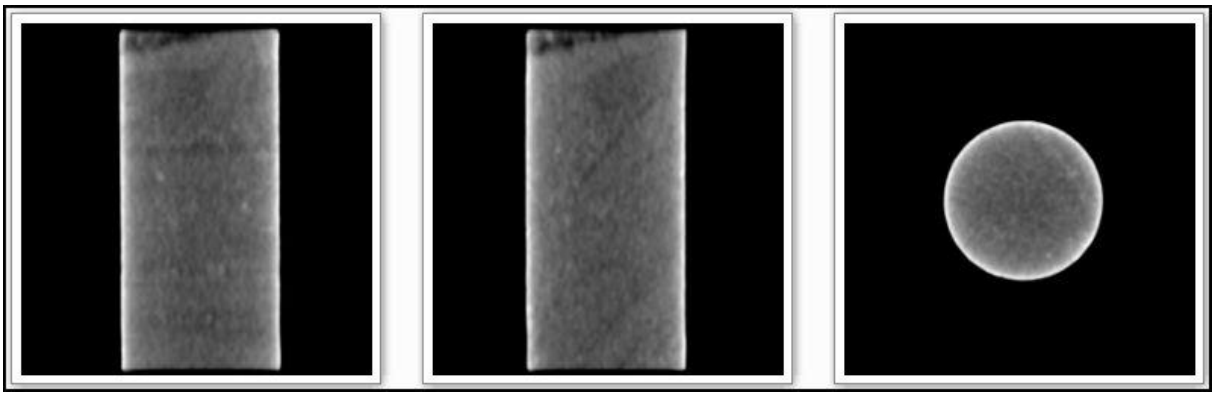

Figure A1.26: CT scans of post-tes sample MGT3-6B

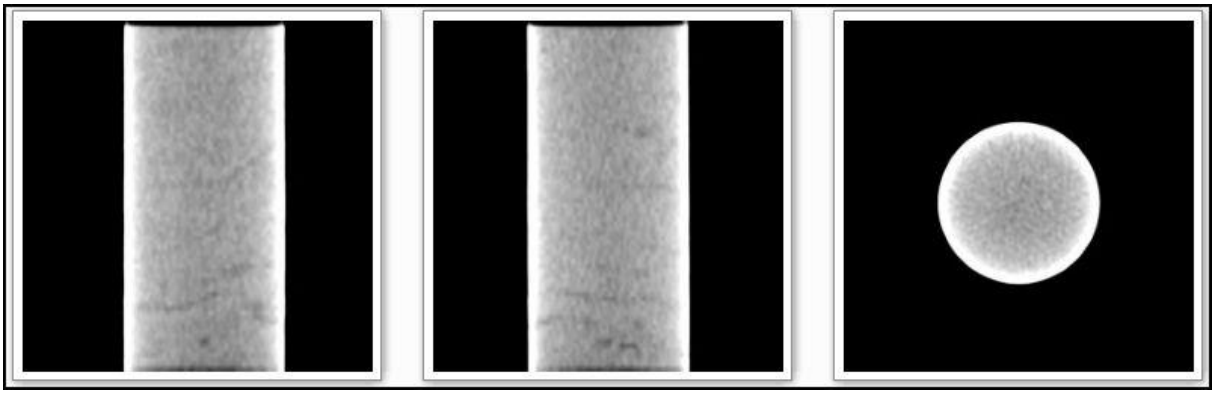

Figure A1.27: CT scans of pre-test samples MGT3-7B

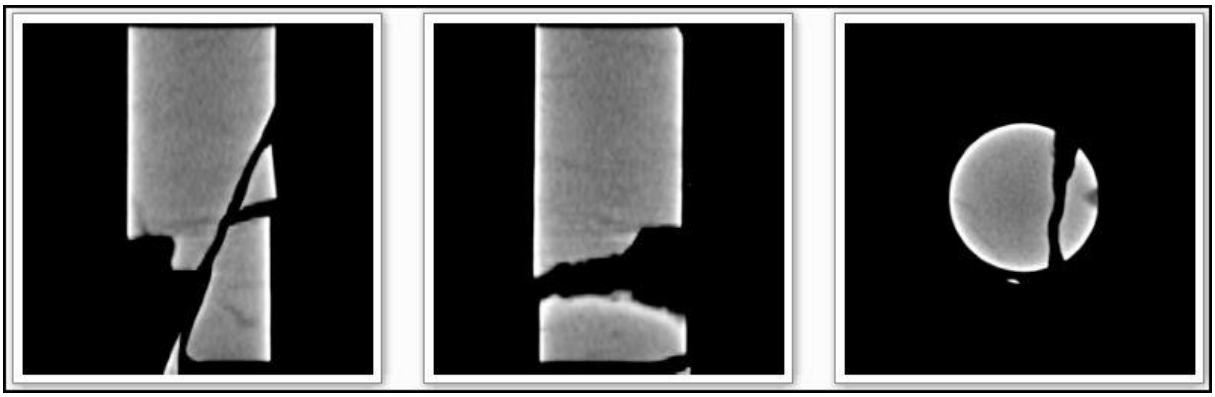

Figure A1.28: CT scans of post-test sample MGT3-7B

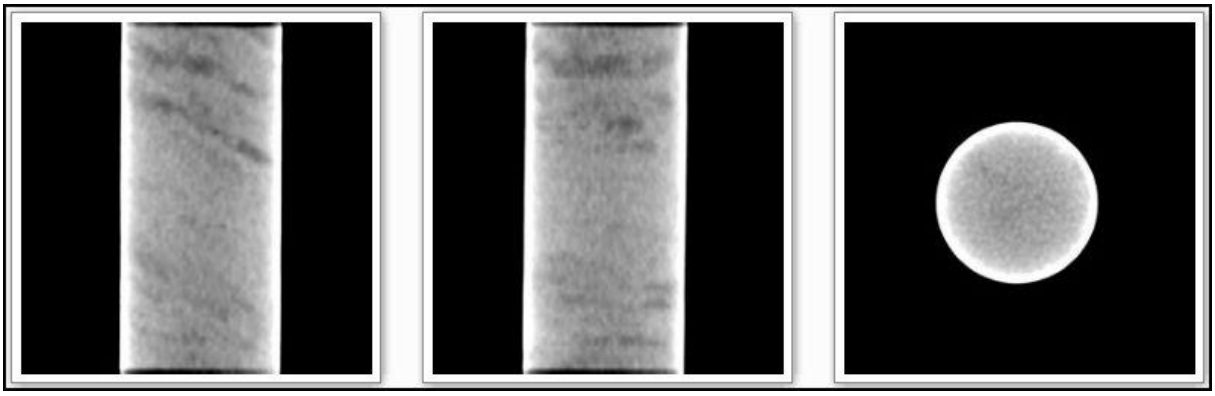

Figure A1.29: CT scans of pre-test sample MGT3-10A

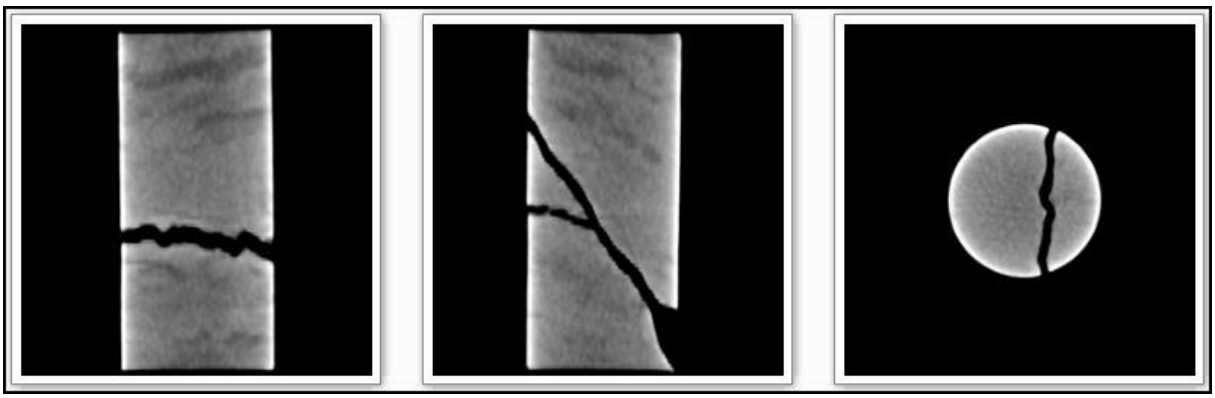

Figure A1.30: CT scans of post-test sample MGT3-10A

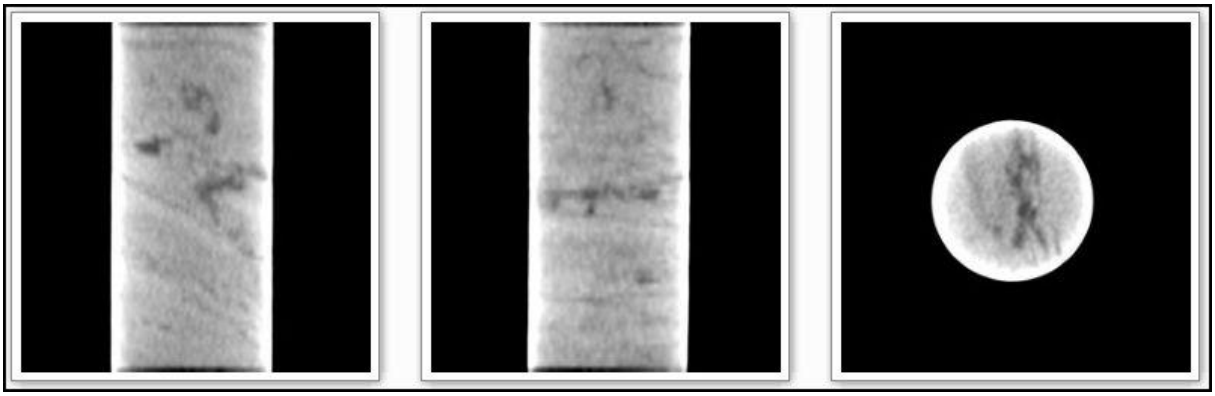

Figure A1.31: CT scans of pre-test sample MGT3-12A

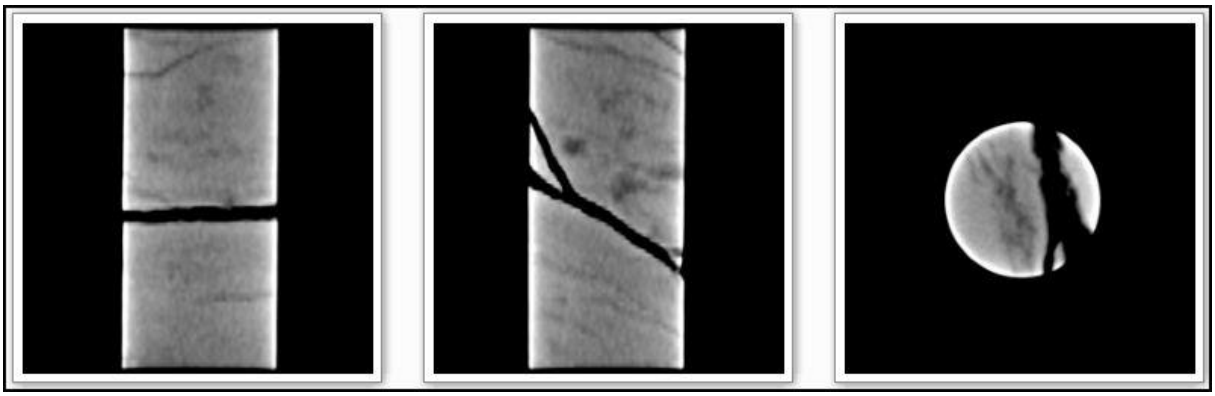

Figure A1.32: CT scans of post-test sample MGT3-12A

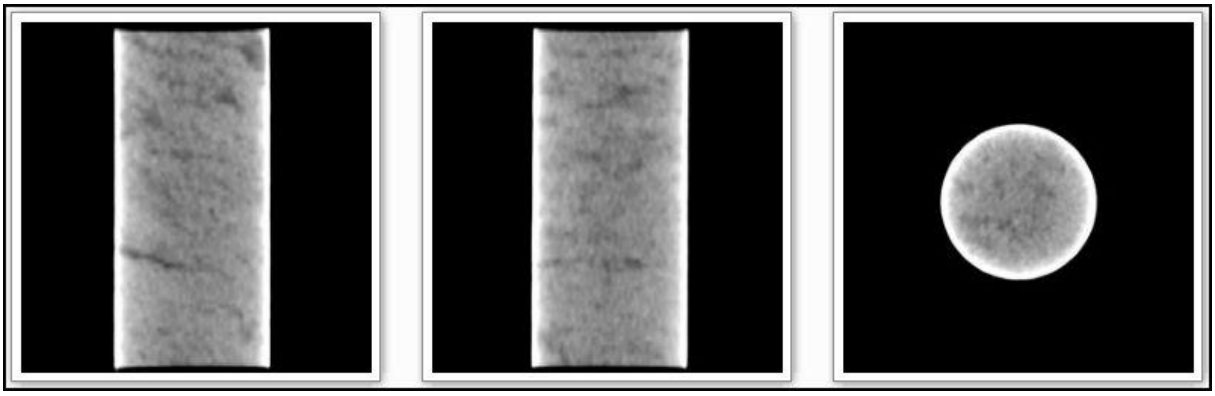

Figure A1.33: CT scans of pre-test sample MGT3-17A

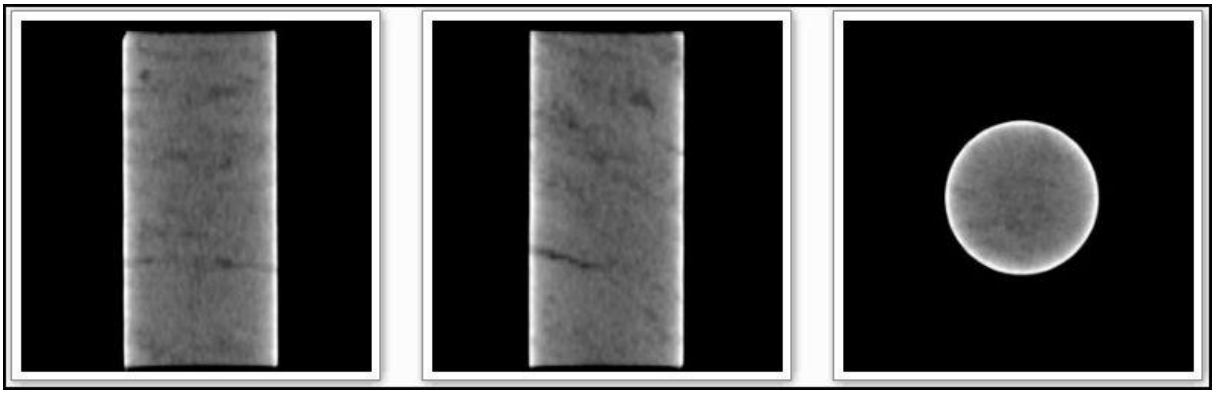

Figure A1.34: CT scans of post-test MGT3-17A

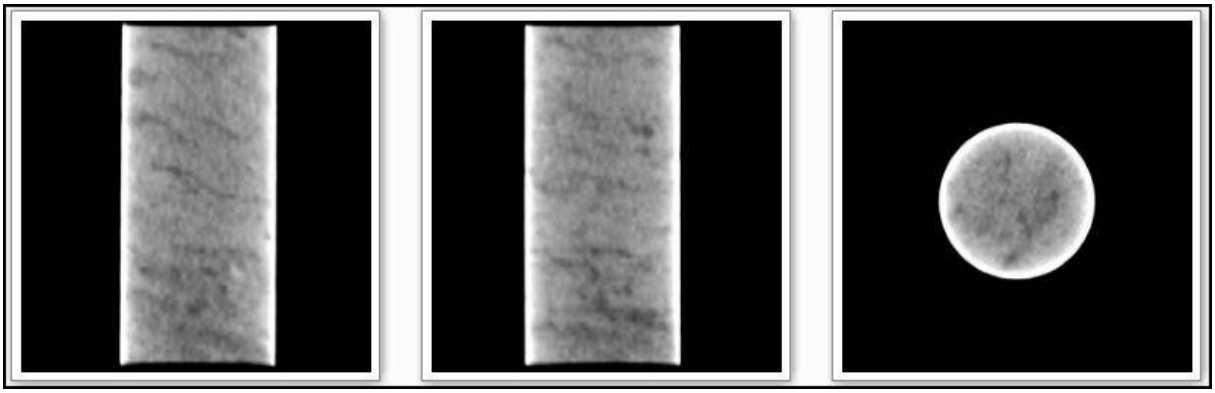

Figure A1.35: CT scans of pre-test samples MGT3-17B

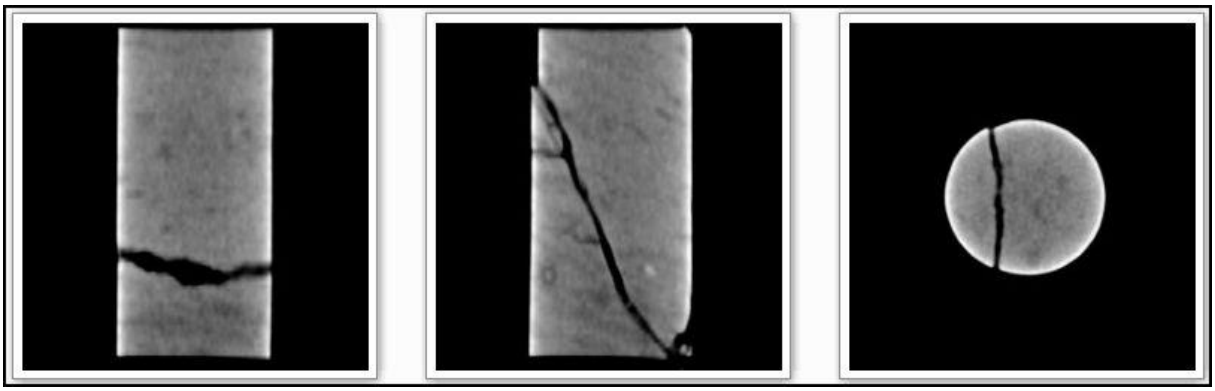

Figure A1.36: CT Scans of post-test sample MGT3-17B

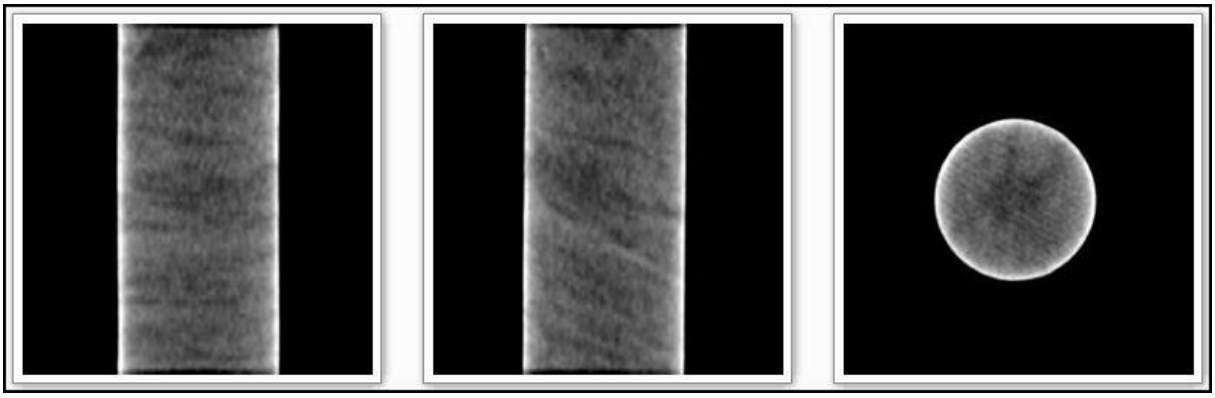

Figure A1.37: CT scans of pre-test sample MGT3-18A

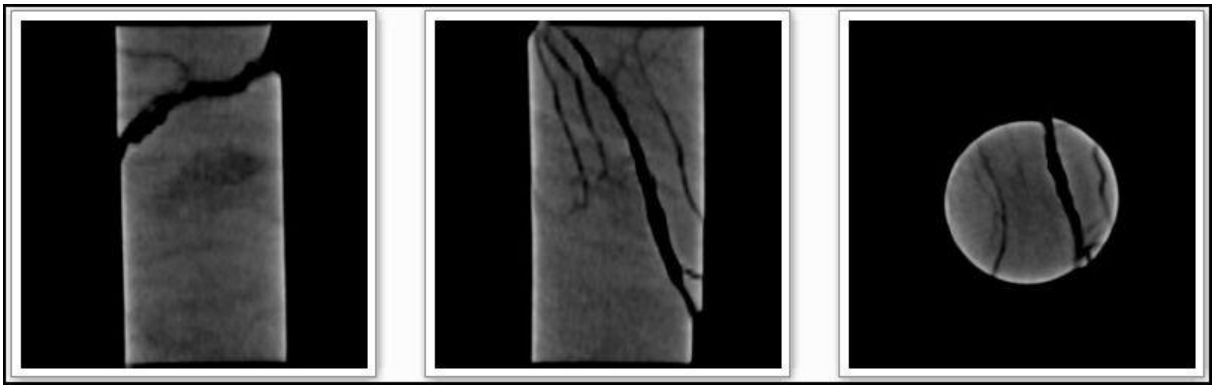

Figure A1.38: CT scans of post-test sample MGT3-18A

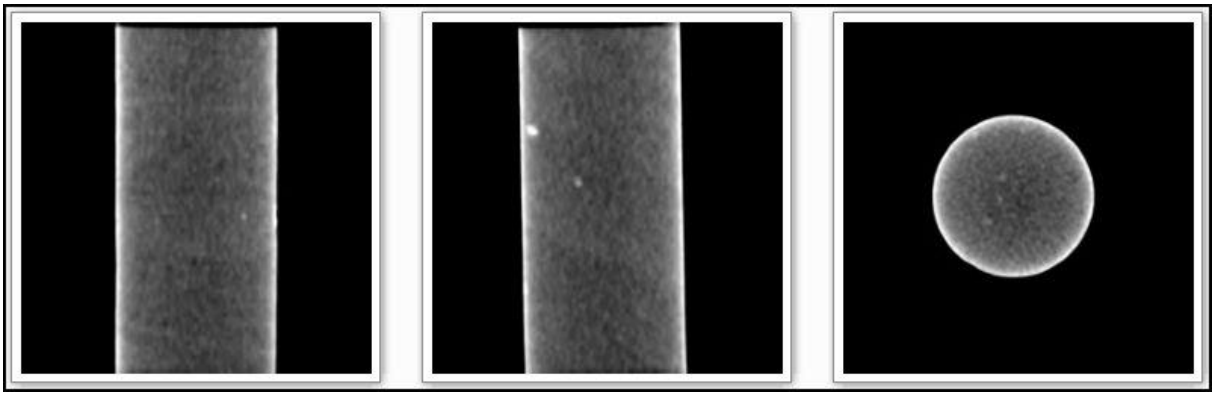

Figure A1.39: CT scans of pre-test sample MGT3-20A

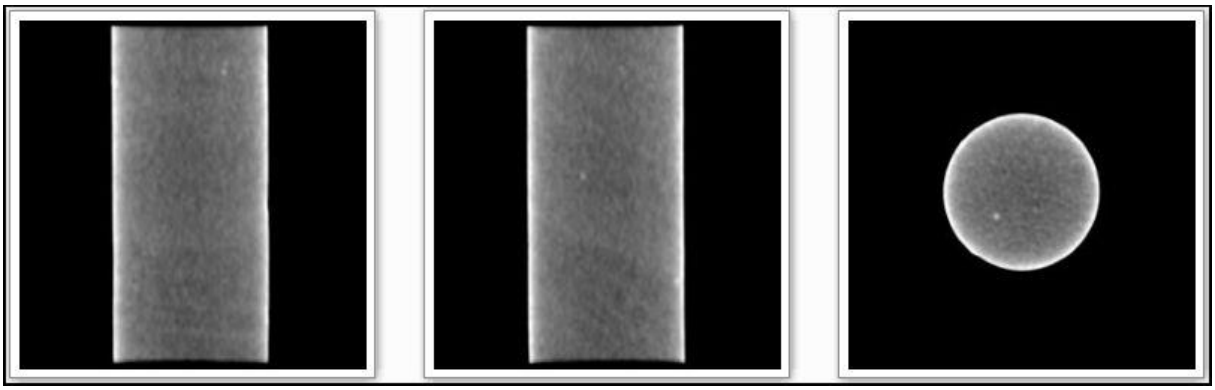

Figure A1.40: CT scans of post-test sample MGT3-20A

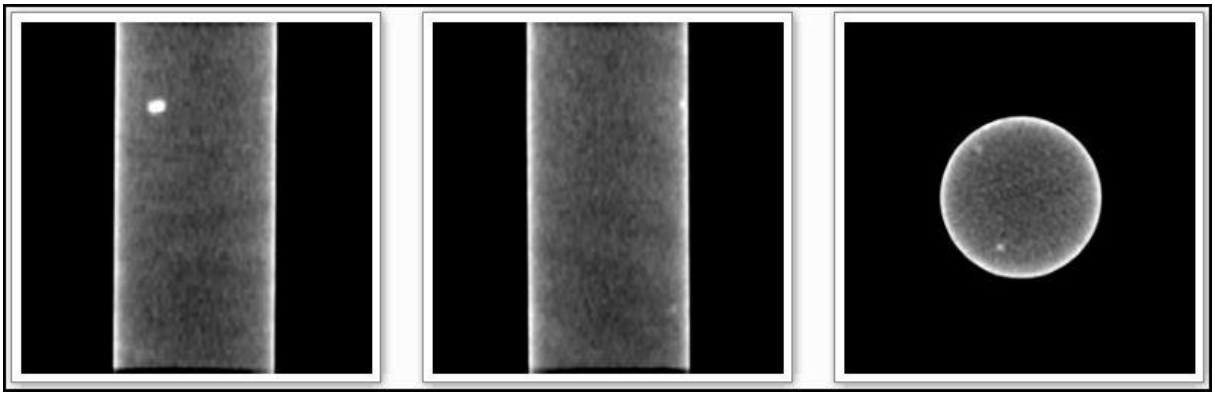

Figure A1.41: CT scans of pre-test sample MGT3-20B

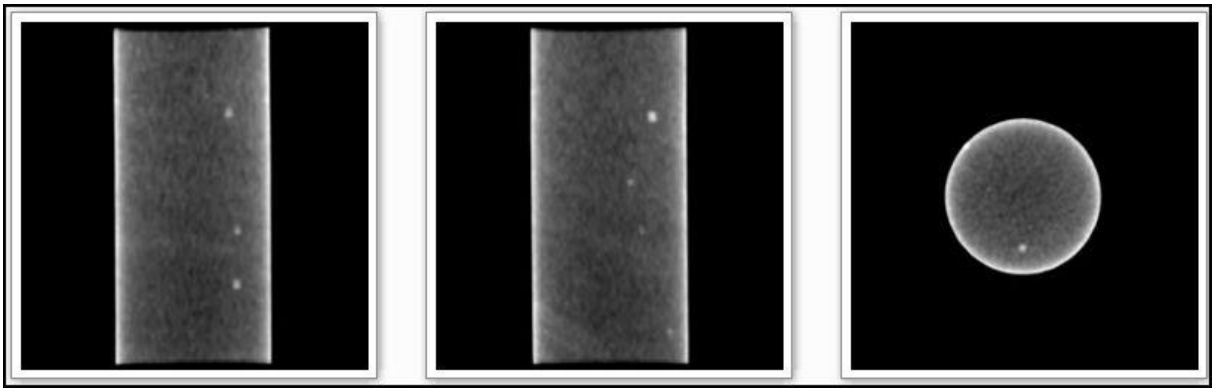

Figure A1.42: CT scans of post-test sample MGT3-20B

Appendix 2. Test results.

In this appendix, the results from the individual tests are given.

sample MGT3-2A					
Stage	C_m . MPa^{-1}	Young's modulus GPa	Poisson's ratio -	Bulk modulus GPa	depletion constant gamma -
Isostatic loading				2.6	
triaxial load		16.3	0.08		
PPD step 470 - 370 bar	4.43E-05	22.6	0.11		0.87
PPD step 370 - 270 bar	4.94E-05	20.2	0.12		0.86
PPD step 270 - 170 bar		15.2	0.10		0.87
PPD step 170 - 70 bar	8.32E-05	12.0	0.11		0.87
PPD step 470 - 70 bar	5.99E-05	16.7	0.10		0.87
PPI step 70 - 470 bar	2.82E-05	35.4	0.22		0.69
PPD step 470 - 70 bar	3.11E-05	32.2	0.22		0.69

Figure A2.1: Sample MGT3-2A test results

Sample MGT3-2B (3811.81 m)				
Stage	C_m MPa^{-1}	Young's modulus GPa	Poisson's ratio -	depletion constant gamma -
triaxial load		15.8	0.07	
PPD 570 - 30 bar	4.29E-05	23.3	0.09	0.90
PPI 30 - 570 bar	3.16E-05	31.6	0.15	0.82
PPD end 570 - 30 bar	3.38E-05	29.6	0.16	0.81

Figure A2.2: Sample MGT3-2B test results

Sample MGT3-3B (3812.72 m)					
Stage	Cm	Young's modulus	Poisson's ratio	Bulk modulus	depletion constant gamma
	.MPa^{-1}	GPa	-	GPa	-
Isostatic load 1st				2.0	
Isostatic unload				8.4	
Isostatic load 2nd				7.3	
triaxial load		17.1	0.07		
PPD step 470 - 170 bar	4.37E-05	22.9	0.05		0.95
PPI step 170 - 470 bar	3.12E-05	32.1	0.12		0.85
PPD step 470 - 170 bar	3.24E-05	30.9	0.11		0.85

Figure A2.3: Sample MGT3-3B test results.

Sample MGT3-4A (3815.49 m)				
Stage	Young's modulus	Poisson's ratio	Bulk modulus	depletion constant gamma
	GPa	-	GPa	-
Isostatic 1			2.3	
triaxial load	12.3	0.10		
PPD step 470 - 170 bar	15.2	0.07		0.90
PPI step 170 - 470 bar	29.7	0.14		0.80
PPD step 470 - 170 bar	27.2	0.14		0.79

Figure A2.4: Sample MGT3-4A test results.

Sample MGT3-4C (3815.49 m)				
Stage	C_m	Young's modulus	Poisson's ratio	depletion constant gamma
	MPa^{-1}	GPa	-	-
triaxial load		5.2	0.05	
PPD 570 - 30 bar	1.24E-04	8.1	0.16	0.81
PPI 30 - 570 bar	5.74E-05	17.4	0.20	0.76
PPD end 570 - 30 bar	6.51E-05	15.4	0.20	0.75

Figure A2.5: Sample MGT3-4C test results.

sample MGT3-6B (3777.05 m)				
Stage	C_m MPa^{-1}	Young's modulus GPa	Poisson's ratio -	depletion constant gamma -
Triaxial loading		10.2	0.09	
PPD1	5.52E-05	18.1	0.13	0.83
PPD2	2.59E-05	38.7	0.11	0.85

Figure A2.6: Sample MGT3-6B test results.

Sample MGT3-7B (3779.71 m)					
Stage	C_m $.10^{-3}$ MPa^{-1}	Young's modulus GPa	Poisson's ratio -	Bulk modulus GPa	depletion constant gamma -
Isostatic 1				1.0	
triaxial load		8.7	0.01		
PPD step 570 - 470 bar	8.64E-02	11.6	-		1.00
PPD step 470 - 370 bar	7.93E-02	12.5	0.04		0.94
PPD step 370 - 270 bar	8.89E-02	11.2	0.06		0.92
PPD step 270 - 170 bar	1.23E-01	5.2	0.34		0.40
PPD step 170 - 70 bar	3.02E-01	1.6	0.40		0.24
PPD step 70 - 53 bar	8.41E-02	10.7	0.20		0.71

Figure A2.7: Sample MGT3-7B test results.

Sample MGT3-10A (3805.42 m)					
Stage	C_m MPa^{-1}	Young's modulus GPa	Poisson's ratio -	Bulk modulus GPa	depletion constant gamma -
Isostatic load				1.2	
triaxial load		8.4	0.02		
PPD step 570 - 470 bar	7.90E-05	12.7	0.02		0.96
PPD step 470 - 370 bar	7.40E-05	13.5	0.08		0.89
PPD step 370 - 270 bar	7.16E-05	14.0	0.10		0.85
PPD step 270 - 170 bar	7.21E-05	13.9	0.15		0.79

Figure A2.8: Sample MGT3-10A test results.

MGT3-12A (3812.47 m)					
Stage	C_m $.10^{-3}$ MPa^{-1}	Young's modulus GPa	Poisson's ratio -	Bulk modulus GPa	depletion constant gamma -
Isostatic load				1.5	
triaxial load		6.6	-		
PPD step 570 - 470 bar	9.35E-02	10.7	0.01		0.98
PPD step 470 - 370 bar	8.23E-02	12.1	0.05		0.93
PPD step 370 - 270 bar	1.32E-01	6.4	0.24		0.63
PPD step 270 - 170 bar	8.42E-02	10.0	0.24		0.62
PPD step 170 - 70 bar	7.48E-02	11.3	0.24		0.63
PPD step 70 - 30 bar	7.25E-02	12.3	0.20		0.70

Figure A2.9: Sample MGT3-12A test results.

MGT3-17A (3807.34 m)					
Stage	C_m $.10^{-3}$ MPa^{-}	Young's modulus GPa	Poisson's ratio -	Bulk modulus GPa	depletion constant gamma -
Isostatic load				3.2	
triaxial load		10.0	-		
PPD step 570 - 470 bar	7.28E-02	13.6	0.06		0.92
PPD step 470 - 370 bar	6.12E-02	15.9	0.10		0.86
PPD step 370 - 270 bar	5.89E-02	16.2	0.13		0.81
PPD step 270 - 170 bar	5.80E-02	15.9	0.17		0.74

Figure A2.10: Sample MGT3-17A test results.

MGT3-17B (3807.34 m)					
Stage	C_m $.10^{-3}$ MPa^{-}	Young's modulus GPa	Poisson's ratio -	Bulk modulus GPa	depletion constant gamma -
isostatic load				1.3	
triaxial load		8.1	-		
PPD step 570 - 470 bar	7.90E-02	12.6	0.02		0.96
PPD step 470 - 370 bar	6.95E-02	14.2	0.08		0.89
PPD step 370 - 270 bar	7.00E-02	14.0	0.09		0.87
PPD step 270 - 170 bar	7.13E-02	13.6	0.11		0.84
PPD step 170 - 135 bar	6.66E-02	10.8	0.31		0.46
PPD step 110 - 70 bar	2.63E-01	1.6	0.41		0.17
PPD step 70 - 30 bar	5.25E-02	15.8	0.25		0.60

Figure A2.11: Sample MGT3-17B test results.

Sample MGT3-18A (3785.22 m)				
Stage	C_m $10^{-3}.MPa^{-1}$	Young's modulus GPa	Poisson's ratio -	depletion constant gamma -
triaxial load		11.6	0.02	
PPD step 570 - 470 bar	6.33E-2	15.6	0.07	0.90
PPD step 470 - 370 bar	5.07E-2	19.4	0.08	0.88
PPD step 370 - 270 bar	4.48E-2	21.9	0.09	0.87
PPD step 270 - 170 bar	4.59E-2	21.2	0.10	0.85
PPD step 170 - 70 bar	5.42E-2	17.8	0.12	0.83
PPD step 70 - 30 bar	4.97E-2	18.6	0.17	0.74
PPI step 30 - 70 bar	3.26E-02	26.2	0.23	0.63
PPI step 70 - 170 bar	2.63E-02	34.8	0.18	0.73
PPI step 170 - 270 bar	3.20E-02	29.2	0.16	0.76
PPI step 270 - 370 bar	3.45E-02	27.2	0.15	0.77
PPI step 370 - 470 bar	4.21E-02	22.6	0.14	0.79
PPI step 470 - 570 bar	5.03E-02	19.1	0.12	0.82

Figure A2.12: Sample MGT3-18A test results.

Sample MGT3-20A (3801.45 m)				
Stage	C_m $.MPa^{-1}$	Young's modulus GPa	Poisson's ratio -	depletion constant gamma -
triaxial load		11.7	0.03	
PPD step 570 - 470 bar	5.69E-02	17.2	0.09	0.87
PPD step 470 - 370 bar	3.70E-02	26.6	0.08	0.88
PPD step 370 - 270 bar	2.82E-02	36.9	0.07	0.88
PPD step 270 - 170 bar	2.82E-02	34.9	0.07	0.87
PPD step 170 - 70 bar	2.61E-02	37.3	0.09	0.85
PPD step 70 - 30 bar	2.05E-02	43.9	0.19	0.70
PPD step 30 - 70 bar	2.05E-02	42.1	0.19	0.66

Figure A2.13: Sample MGT3-20A test results.

Sample MGT3-20B (3801.45 m)					
Stage	C_m $.10^{-3}.MPa^{-}$	Young's modulus GPa	Poisson's ratio -	Bulk modulus GPa	depletion constant gamma -
isostatic load				1.6	
triaxial load		11.8	0.02		
PPD step 570 - 470 bar	5.83E-02	17.0	0.07		0.90
PPD step 470 - 370 bar	3.33E-02	29.7	0.06		0.90
PPD step 370 - 270 bar	2.90E-02	34.2	0.05		0.90
PPD step 270 - 170 bar	2.67E-02	37.1	0.06		0.89
PPD step 170 - 70 bar	2.98E-02	33.2	0.06		0.89
PPD step 70 - 30 bar	1.74E-02	56.0	0.09		0.83

Figure A2.14: Sample MGT3-20A test results.

Appendix 3. Experimental setup

The triaxial and rock physics experiments are performed with a triaxial compaction apparatus (called Ultrasound Velocity Cell (UVC) cell).

A schematic diagram of the UVC is shown in the Figure A2.1. A cylindrical sample is mounted on titanium end caps and enclosed in an impermeable 2.5 mm-thick Viton® sleeve. The sample is mounted inside a 1000 bar capacity pressure vessel with an integral axial loading piston.

The sample is loaded axially by applying a fluid pressure in the chamber at the bottom of the loading piston using a piston (hydraulic) actuator. The pressure is measured using a 1000 bar pressure gauge and controlled to within 1 bar by a custom analog servo- controller. Radial stress is applied directly to the sample through oil pressure on the elastomer sleeve using a similar piston (hydraulic) actuator, pressure gauge, and controller. No pore-fluid pressure is applied, because of the very low porosity and permeability. The sample in- and outlet was kept at ambient pressure. This doesn't mean that the internal pore pressure is also ambient, but this can't be recorded.

Changes in the sample length are measured using the relative vertical displacement of two INVAR rods in contact with the end caps through concentric bores drilled in the bottom piston and top plate of the pressure vessel. A rectangular INVAR frame, suspended independently of the vessel, transmits the relative movement of the rods to a linear variable displacement transducer (LVDT) located beneath the pressure vessel. In this way, the axial shortening and extension of the sample plus end caps is measured.. During processing, the raw axial displacement data are corrected for the axial deformation of the end caps due to axial and radial loads and temperature changes. The change in the diameter of the sample is measured using a strain-gauged cantilever bridge. The bridge is positioned at the centre of the sample. The sensor is clamped onto two pins that pierce the elastomer sleeve, making direct contact with the sample at opposite sides. During loading under uniaxial constant-lateral strain conditions, the total radial stress is varied to maintain a constant radial dimension using the above-mentioned servo-controller, and include corrections for pressure effects on the radial sensor. Calibration experiments on aluminium samples show that the radial displacement under uniaxial constant-strain conditions can be maintained within ± 1 microns (± 0.05 millistrain).

Data acquisition and test sequence control are carried out by custom software operating on a PC.

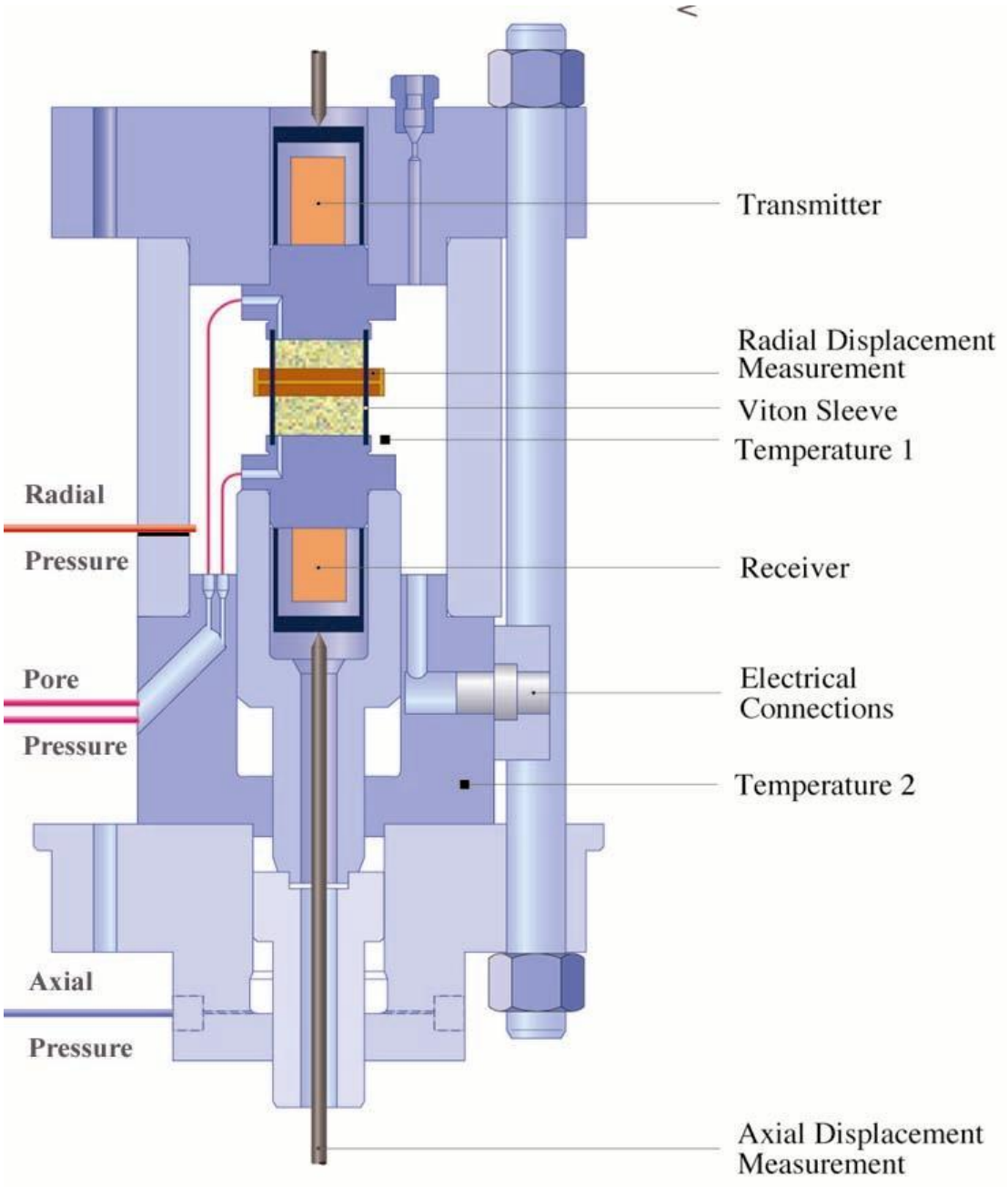

Figure A2.1: Schematic diagram of the UVC triaxial cell.

Bibliographic information

Classification	Restricted
Report Number	SR.15.11616
Title	Geomechanical experiments on Ten Boer rock samples from well Moddergat-3
Author(s)	A.J. van der Linden (PTI/RF) P.M.M. Zuiderwijk (PTI/RF) S. Hol (PTI/RF) F. Marcelis (PTI/RF) A.H. Coorn (PTI/RF)
Keywords	Geomechanics, Moddergat-3, Nes, Ten Boer, shale, cap rock, Wadden, Groningen, gas, experiments, compaction, compression, subsidence, constitutive behaviour, poroelasticity, uniaxial, depletion
Date of Issue	July 2015
US Export Control	Non US - Non Controlled
Reviewed by	A. Makurat (PTI/RF)
Approved by	H. de Jong (PTI/RF)
Sponsoring Company / Customer	NAM
Issuing Company	Shell Global Solutions International B.V. P.O. Box 60 2280 AB Rijswijk The Netherlands

Report distribution

Electronic distribution (PDF)

Name, Company, Ref. Ind. *PDF*

PT Information Services, PTT/TIKE, PT-Information-Services@Shell.com

Baehr, Hermann NAM-PTU/E/G

Bierman, Stijn M GSNL-PTD/TASE

van den Bogert, Peter AJ GSNL-PTU/E/Q

van Boom, Ruud, NAM-UIO/T/DL

Bourne, Stephen J GSNL-PTI/RC

Coorn, Ab H GSNL-PTI/RF

Doornhof, Dirk NAM-PTU/E/Q

Dudley, John W SIEP-PTI/RF

van Eijs, Rob MHE NAM-PTU/E/Q

Hol, Sander GSNL-PTI/RF

Hoogerduijn-Strating, Eilard H NAM-UIO/T/DL

Jansen, Jeroen M NAM-UIO/T/H

de Jong, H SIEP-PTI/RF

Kole, Pepijn R NAM-PTU/E/Q

Kraaijeveld, Famke GSNL-PTI/RC

Makurat, Axel GSNL-PTI/RF

Marcelis, Fons H M GSNL-PTI/RF

Mossop, Anthony P GSNL-PTI/RC

van der Linden, Arjan J GSNL-PTI/RF

Park, Timothy A GSUK-PTD/TASE

Post, Alice D PTIN-PTU/I/S

Schutjens, Peter GSNL-PTU/E/Q

van der Veen, Wim NAM-PTU/E/G

van der Wal, Onno NAM-PTU/E/Q

Wentinck, Rick M GSNL-PTI/RC

Wong, Sau-Wai SIEP-PTI/U

Zuiderwijk, Pedro M M GSNL-PTI/RF